Next Generation Die Design for Biomass Pelleting

Nielsen, Simon Klinge

Publication date:
2020

Document Version
Publisher's PDF, also known as Version of record

NEXT GENERATION DIE DESIGN FOR BIOMASS PELLETING

BY
SIMON KLINGE NIELSEN

DISSERTATION SUBMITTED 2020

AALBORG UNIVERSITY
DENMARK

Next Generation Die Design for Biomass Pelleting

Ph.D. Dissertation

Simon Klinge Nielsen

Dissertation submitted August, 2020

Dissertation submitted: August, 2020

University PhD Supervisor: Associate Professor Matthias Mandø
Aalborg University

Company PhD Supervisor: Engineering Manager Andreas B. Rosenørn
Andritz Feed & Biofuel

PhD committee: Associate Professor Henrik Sørensen (chairman)
Aalborg University

Lead Chemistry Specialist Jens Kai Holm
Markets & Bioenergy, Ørsted

Professor Sylvia Larsson
Swedish University of Agricultural Sciences

PhD Series: Faculty of Engineering and Science, Aalborg University

Department: Department of Energy Technology

ISSN (online): 2446-1636
ISBN (online): 978-87-7210-684-7

Published by:
Aalborg University Press
Kroghstræde 3
DK – 9220 Aalborg Ø
Phone: +45 99407140
aauf@forlag.aau.dk
forlag.aau.dk

Printed in Denmark by Rosendahls, 2020

Abstract

The production of biomass pellets involves different design- and process parameters of the pellet press, which affect the pellet properties and the operational expense of the pellet production. In the pellet press, the feedstock is compressed and converted from sawdust into solid pellets. The die has to be custom designed for each production site due to the different properties of the feedstock used. The design of dies is partly relying on experiences from trial-and-error processes, which may involve several design iterations before the final design is developed.

The die design is correlated to the pelleting pressure, which is determined by the friction between the pellet and the die. Typical problems with dies are either that the pelleting pressure is too low to produce pellets with the required density and mechanical durability, or the pelleting pressure becomes too high. High pelleting pressure reduces the lifetime of the die and increases the power consumption of the pellet press. In case that the pelleting pressure becomes too high, the feedstock blocks the die and causes a time-consuming shutdown of the pellet press.

In this thesis, existing pelleting studies are reviewed, and experimental, and modeling studies of the physical processes in the die are performed, to obtain a better understanding of the design parameters of the die, and how these affect the pelleting process.

An extensive literature study shows that design and process parameters, such as the press channel inlet, die area, die speed, and gap size between die and roller, are rarely considered in pelleting studies. However, a few studies indicate that these parameters have a significant effect on energy consumption, and also affect the pellet durability. The literature study also shows that the existing methods for calculating the pelleting pressure in the die's press channels are based on a set of equations that only apply for calculation of a pure cylindrical press channel.

A 1D model is developed for calculating the pelleting pressure in press channels with a conical inlet section, and experimental single pelleting tests are performed for validation of the model. Simulations of the pressure contours in press channels show that the peak pressure is located where the

conical inlet meets the cylindrical channel, which also is where the wear of the channel is most pronounced. In addition to the pelleting pressure, the presented model is set up to calculate the feedstock density and the mass-specific energy consumption of the pelleting process.

Further investigation of the press channel inlet is performed by using a novel experimental method for analyzing the feedstock motion in the press channel, and by setting up a Computational Fluid Dynamics model for simulating the feedstock flow. The analyzes of feedstock motion in the press channel show that the conical inlet design of the press channel affects the shape of the feedstock layers in pellets, which is shown to correlate with the pellet durability. The analyzes also show cases of stagnant feedstock on the die surface and in the press channel inlet.

A pilot-scale pellet press is set up for experimental testing, where the thickness of the feedstock layer on the die surface and the gap size between die and roller are investigated. The results show that the energy consumption of the pellet press decreases, and the pellet durability increases when the thickness of the feedstock layer on the die is increased. The test results of the gap size between die and roller show that the energy consumption increases and the pellet durability decreases when the gap size is increased. Hence, the thickness of the feedstock layer on the die and the gap size between die and roller are found to be important process parameters in the pellet press.

The mechanical behavior of biomass feedstock is studied via constitutive modeling and experimental compression tests. The results of the constitutive modeling show that the viscoplastic behavior of compressed biomass can be modeled using an SLS Maxwell model, with two strain-hardening springs and a dashpot. The coefficients of the model elements are shown to correlate with the energy that is required for compressing the biomass, while the model's dashpot work is lowest for pellets produced with small particles, which also have the highest durability measured from the experiments.

Resumé

Produktionen af biomasse piller indbærer forskellige design- og procesparametre af pillepressen, som påvirker pillernes egenskaber og produktionsomkostningerne. I pillepressen bliver råvaren komprimeret og omsat fra savsmuld til solide træpiller. Designet af matricen skal tilpasses specifikke produktionssteder, grundet forskelle i råvareegenskaber. Matricedesignet er til dels baseret på erfaringer ved at prøve sig frem, hvilket kan betyde op til flere designiterationer før et passende matricedesign er udviklet.

Matricedesignet korrelerer med pelleteringstrykket, som afhænger af friktionen mellem pillen og matricen. Typiske problemer med matricer er at pelleteringstrykket enten er for lavt til at kunne producere piller med den påkrævede densitet og sammenhængskraft, eller at pelleteringstrykket er for højt. Højt pelleteringstryk reducerer holdbarheden af matricen og øger energiforbruget af pillepressen. I tilfælde af at pelleteringstrykket bliver for højt, blokeres matricen af råvaren og forårsager et tidskrævende driftsstop af pillepressen.

I denne afhandling er eksisterende pelleteringsstudier gennemgået samt eksperimentelle og modelleringsstudier af de fysiske processer i matricen er foretaget, for at opnå en bedre forståelse af matricens designparametre, og hvordan disse påvirker pelleteringsprocessen. Et grundigt litteraturstudie viser at design- og procesparametre, såsom pressekanalens indløb, matrice areal, matrice hastighed og afstanden mellem matrice og rulle sjældent er betragtet i pelleteringsstudier. Dog har enkelte studier vist at disse parametre har en signifikant effekt på energiforbruget, og samtidig påvirker pillernes sammenhængskraft. Litteraturstudiet viser også at de eksisterende metoder til at beregne pelleteringstrykket i pressekanaler er baseret på et sæt ligninger, som er begrænset til beregning for en cylindrisk pressekanal.

En 1D model er blevet udviklet for at beregne pelleteringstrykket i pressekanaler med et konisk indløb, og eksperimentelle enkeltpelleteringsforsøg er blevet udført til validering af modellen. Simuleringer af trykkonturerne viser at det højeste tryk er i overgangen mellem det koniske indløb og den cylindriske del af pressekanalen, hvilket også er her at sliddet af kanalen er koncentreret. Ud over pelleteringstrykket, er den præsenterede model sat op

til at beregne råvaredensiteten og det massespecifikke energiforbrug.

Videre undersøgelse af pressekanalens indløb er udført med en ny eksperimentel metode til at analysere råvarens bevægelse i pressekanalen, og ved at opsætte en Computational Fluid Dynamics model til at simulere råvarestrømningen. Analyserne af råvarestrømning i pressekanalen viser at koniske indløbsdesign påvirker formen af råvarelagene i piller, hvilke er påvist at korrelere med pillernes sammenhængskraft. Analyserne viser også tilfælde med stillestående råvare på matricens overflade og i indløbet af pressekanalen.

En pilotskala pillepresse er blevet opstillet til eksperimentel test, hvor lagtykkelsen af råvaren på matriceoverfladen og afstanden mellem matrice og rulle er blevet undersøgt. Resultaterne af testene viser at energiforbruget af pillepressen falder, og pillernes sammenhængskraft stiger, når lagtykkelsen af råvaren på matricen forøges. Testresultaterne af afstanden mellem matrice og rulle viser at energiforbruget stiger, og pillernes sammenhængskraft falder, når afstanden forøges. Dermed er lagtykkelsen af råvaren på matricen samt afstanden mellem matrice og rulle påvist at være vigtige procesparametre i pelletpressen.

De mekaniske egenskaber af biomasse er undersøgt via konstitutiv modellering og eksperimentelle kompressionstests. Resultaterne af den konstitutive modellering viser, at de visko-plastiske egenskaber af komprimeret biomasse kan modelleres med en SLS Maxwell model, med to tøjningsstivende fjedre og en dæmper. Modellens elementkoefficienter er påvist at korrelere med energien, der er påkrævet til at komprimere biomassen, mens at dæmperarbejdet i modellen er lavest for piller produceret med små partikler, hvilke også har den højeste sammenhængskraft målt i eksperimenterne.

Contents

Thesis Details

Thesis Title:	Next Generation Die Design for Biomass Pelleting
Ph.D. Student:	Simon Klinge Nielsen
Supervisors:	Associate Professor Matthias Mandø, Aalborg University Engineering Manager Andreas B. Rosenørn, Andritz Feed & Biofuel

The body of the thesis consists of the following papers:

[A] S. K. Nielsen, M. Mandø, A. B. Rosenørn, "1D Model for Investigation of Energy Consumption and Wear in Die Designs Used for Biomass Pelleting", *Proceedings of the* 26^{th} *European Biomass Conference and Exhibition, Copenhagen, Denmark, May 14-17*, pp. 550-558, 2018, `https://doi.org/10.5071/26thEUBCE2018-2CO.13.1`.

[B] S. K. Nielsen, M. Mandø, A. B. Rosenørn, "Review of Die Design and Process Parameters in the Biomass Pelleting Process", *Powder Technology*, Vol. 364, pp. 971-985, 2020, `https://doi.org/10.1016/j.powtec.2019.10.051`

[C] S. K. Nielsen, H. Rezaei, M. Mandø, S. Sokhansanj, "Constitutive Modelling of Compression and Stress Relaxation in Pine Pellets, *Biomass & Bioenergy*, Vol. 130, no. 105370, 2019, `https://doi.org/10.1016/j.biombioe.2019.105370`

[D] S. K. Nielsen, M. Mandø, "Experimental and Numerical Investigation of Die Designs in Biomass Pelleting and the Effect on Layer Formation in Pellets", 2020, *submitted to Biosystems Engineering (revised version under review).*

[E] S. K. Nielsen, M. Mandø, A. B. Rosenørn, "Experimental Investigation of Feedstock Layer Thickness and Die-Roller Gap in Wood Pelleting", *Proceedings of the World Sustainable Energy Days, Wels, Austria, March 4-6*, pp. 1-10, 2020.

Preface

This thesis is submitted as a collection of papers in fulfillment of the requirements for the degree of Doctor of Philosophy at the Department of Energy Technology, Aalborg University, Denmark. The Ph.D. project is a part of the Industrial Ph.D. program by Innovation Fund Denmark under File No. 7038-00016B, with Andritz Feed & Biofuel and Aalborg University as the project partners. Andritz is a global manufacturer of equipment for pelleting, with an annual production of more than 16.000 dies for pellet presses.

The study has been carried out at Andritz in Esbjerg and the Department of Energy Technology at Aalborg University, Campus Esbjerg. The work was conducted in the period from September 2017 to August 2020 under the supervision of Associate Professor Matthias Mandø and Engineering Manager Andreas Brinch Rosenørn.

During the project, I had a three months stay in the Autumn 2019 as a visiting researcher at the University of British Columbia in Vancouver, Canada, with supervision from Dr. Hamid Rezaei and Professor Shahab Sokhansanj.

I want to thank Andritz for the opportunity of doing this Ph.D. and thanks to my colleagues at Andritz, Aalborg University, and the University of British Columbia for providing a resourceful and enjoyable research environment. Thanks to Application Manager Torben Poulsen for taking me under his wings and giving me the chance to experience industrial pelleting plants, and always providing a technical aspect. Thanks to Service Technician Jens Vester and Automation Engineers Ole Bank and Thomas Jørgensen, for helping with the installation of the pellet press setup. Thanks to Andreas Brinch Rosenørn for providing helpful supervision through the project.

A special thanks to my supervisor Matthias Mandø. Thank you for our many valuable discussions, both on- and off-topic, and for always being supportive and taking the time whenever needed. Also, thanks to Christian Gejl Pedersen, without whom this project never had been established.

Finally, I am grateful for the support of my family and friends. Specially thanks to my girlfriend and son.

Simon Klinge Nielsen
Aalborg University, August 1, 2020

Nomenclature

β	Press channel inlet angle $[^\circ]$
Δt	Time step $[s]$
$\dot{\gamma}$	Shear rate $[1/s]$
$\dot{\gamma}_c$	Critical shear rate $[1/s]$
$\dot{m}$	Mass flow rate $[kg/s]$
ϵ	Strain $[-]$
ϵ_1	Strain of system 1 in the SLS model $[-]$
ϵ_2	Strain of system 2 in the SLS model $[-]$
ϵ_{s2}	Strain of spring 2 in the SLS model $[-]$
η	non-Newtonian viscosity $[Pa \cdot s]$
μ	Viscosity $[Pa \cdot s]$
μ_w	Coefficient of friction $[-]$
ν	Poisson's ratio $[-]$
ω_d	Rotational frequency of the die $[1/s]$
ϕ_s	Solid ratio $[-]$
ϕ_v	Void ratio $[-]$
ρ	Density $[kg/m^3]$
ρ_b	Bulk density $[kg/m^3]$
ρ_s	Density of the solid spring $[kg/m^3]$
σ	Stress $[Pa]$

σ_1	Stress of system 1 in the SLS model $[Pa]$
σ_2	Stress of system 2 in the SLS model $[Pa]$
τ_0	Yield stress $[Pa]$
τ_w	Wall shear stress $[Pa]$
a	Empirical coefficient $[kg]$
A_a	Cross-sectional area of the press channel $[m^2]$
A_r	Area of the press channel wall $[m^2]$
A_d	Area of the die's inner surface $[m^2]$
AR	Ratio of active and transition area to the total surface area of the die $[-]$
D	Press channel diameter $[m]$
E_c	Compression energy $[J]$
E_{1-2}	Spring modulus $[Pa]$
F_p	Pelleting force, static $[N]$
F_r	Radial force $[N]$
F_0	Outlet or initial resistance force $[N]$
F_μ	Friction force $[N]$
F_e	Pelleting force, kinetic $[N]$
F_{rn}	Radial force component acting normal to the die wall $[N]$
F_{rp}	Radial force component acting parallel to the die wall $[N]$
h	Countersink inlet depth $[m]$
h_f	Thickness of the feedstock layer $[m]$
h_{fc}	Thickness of the compressed feedstock layer $[m]$
k_r	Ratio of axial to lateral stress $[-]$
k_{1-3}	Empirical coefficients
L	Press channel length $[m]$
m_f	Mass of the feedstock layer $[kg]$

N	Number of elements $[-]$
n	Element number $[-]$
N_r	Number of rollers in the pellet press $[-]$
N_{ch}	Number of press channels in the die $[-]$
p	Pressure $[Pa]$
P_c	Compression pressure $[Pa]$
P_{No}	Prestressing pressure $[Pa]$
P_p	Pelleting pressure $[Pa]$
P_x	Local pelleting pressure $[Pa]$
r	Radial axis of the press channel $[-]$
T	Temperature $[°C]$
t	Time $[s]$
v	Specific volume $[m^3/kg]$
v_1	Initial specific volume $[m^3/kg]$
v_2	Final specific volume $[m^3/kg]$
v_r	Axial velocity in the press channel $[m/s]$
v_z	Radial velocity in the press channel $[m/s]$
w	Mass-specific energy $[J/kg]$
w_c	Mass-specific compression energy $[J/kg]$
w_μ	Mass-specific friction energy $[J/kg]$
x	Position in the press channel $[m]$
x_e	Position of the press stop $[m]$
x_p	Position for the static pelleting force $[m]$
x_{1-2}	Spring coefficients $[Pa]$
z	Longitudinal axis of the press channel $[-]$
W_μ	Frictional power dissipation $[W]$

Part I

Extended summary

Chapter 1

Introduction

This chapter presents the motivation of this study and brief introduction to the biomass pelleting process. It also presents the main objectives of this work together with an outline of the papers included in the thesis.

1.1 Motivation

The global consumption of wood pellets experiences massive growth, and the production has more than doubled in five years, from 24.9 Mt in 2013 it reached 55.7 Mt in 2018, and is expected to continue increasing [1, 2]. The main reason for the increasing pellet production is due to the replacement of fossil fuels with biofuels, where political initiatives and economic viability are the main drivers of the transition [3]. In the European Union, biomass is foreseen to play an essential role in obtaining the target of 27% renewable energy by 2030 [4, 5]. Also, in Japan and South Korea, the consumption of wood pellets is rapidly increasing due to government initiatives such as the Renewable Portfolio Standard and the Feed-in Tariff [6, 7].

In the supply chain costs for wood pellets, pellet plants are associated with a high Operating Expense (OPEX), and together with the feedstock cost, these are the most expensive parts of the supply chain [8]. For the pellet press itself, the OPEX is mainly based on the electrical power consumption and the maintenance cost to wear parts as dies and rollers [9]. Due to differences in feedstock species, particle size, and process conditions as temperature and moisture content, the design of the pellet press die needs to be fitted to each production site. In the industry, the design of dies is somewhat relying on experiences from trial-and-error processes, where the optimal die should facilitate a low energy consumption while maintaining the production of quality pellets that fulfills the international standards or certifications [10, 11].

Specifying a die for a new production site or a new feedstock may involve

several design iterations before a final die design is developed. The friction between the pellet and the die determines the pelleting pressure. Typical problems with dies are either that the pelleting pressure is insufficient to produce pellets with the required density and mechanical durability, or the pelleting pressure becomes too high. High pelleting pressure decreases the lifetime of the die and rollers and increases the power consumption of the pellet press [12], which increase the OPEX. In case that the pelleting pressure becomes too high, the die blocks and cause a time-consuming shutdown of the pellet press.

1.2 Objectives

The objectives of this project are as follows:

- Obtain a better understanding of the design parameters of the die and how these affect the pelleting process.
- Develop a model that is capable of solving the pelleting pressure and energy consumption in the die, which can be used when designing new dies and may reduce the lead time for designing feedstock-specific dies.
- Identify important process parameters in the pelleting process, which can and lead to reduction of the mass-specific energy consumption of pellet presses.

1.3 The Pelleting Process

The purpose of pelleting is to raise the energy density of the raw material, which lowers the cost for transportation, and to produce pellets with standardized properties for combustion purposes [13, 14]. Figure 1.1 illustrates the processing steps in a typical pellet production and lists the physical properties of the feedstock throughout the process. As shown in figure 1.1, the feedstock is processed before being pelleted, where the feedstock moisture content, particle size, and temperature are adjusted to facilitate production of high quality pellets.

Studies of the pelleting process have shown that the energy consumption for pelleting wood is negatively correlated with feedstock moisture content, whereas an optimum for the mechanical pellet durability is in the range 10-15% [16,17]. The moisture content of the feedstock is adjusted via the drying and conditioning stages shown in figure 1.1.

Hammer mills grind the feedstock particles, to ensure that the particles entering the pellet press are in a size range, where the particles are suitable for pelleting. The particle size affects the durability of the pellets, and the

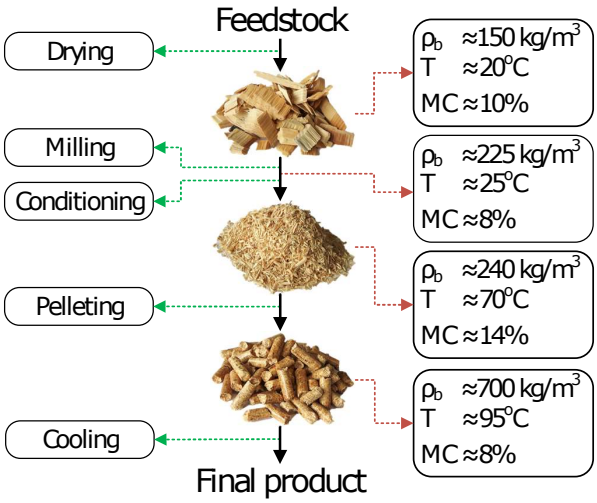

Figure 1.1: Processing of feedstock for pelleting, illustrating the change in feedstock properties during the process. ρ_b is the bulk density, and MC is the moisture content on dry basis (d.b) (figure from paper B [15]).

compressive strength measured from single pellet tests, where particles sizes below 2 mm have shown to produce more durable pellets, and pellets with a higher compressive strength compared to pellets made from larger particle sizes [18,19]. However, the energy required for milling increases when smaller particles are produced, which also reduces the milling capacity. Thus, the degree of size reduction sometimes becomes a tradeoff between producing small particles and mill capacity.

The conditioning process is the final process step of the feedstock before pelleting. The primary purpose of the conditioning is to pre-heat the feedstock by adding steam, and to increase the moisture content before pelleting. Increasing the feedstock temperature to 60-70 °C before pelleting significantly decreases the energy consumption of the pellet press, where the elevated temperature of the feedstock reduces the friction in the die of pellet press [16,20].

The conditioned feedstock is pressed to pellets, which increases the bulk density of the feedstock above 600 kg/m^3 [14]. The specific energy consumption of the pellet press typically is in the range 30–60 kWh/ton dependent on the feedstock properties and pellet press configuration, but for some cases energy consumption exceeds 70-80 kWh/ton [21–24]. The production capacity of industrial-scale pellet presses is in the range from a few tonnes per hour and up to 12 tonnes per hour.

Pellet Press Configuration and Die Design

Pellet presses are based on a die and roller configuration, where the feedstock is compressed between the die and roller. The compression between die and roller presses feedstock into and through press channels in the die. Figure 1.2a shows a ring die with a two-roller configuration, where the arrows indicate the rotational motion of the parts. The press motor drives the die. The rotation of the rollers is caused by friction between the die, the feedstock, and the rollers. The die is designed with press channels oriented normal to the inner die surface. It is in the press channels that the feedstock is pressed into the cylindrical pellet shape. Figure 1.2b illustrates a cross-sectional view of the ring die and roller. In front of the roller, feedstock is distributed in a layer across the inner die surface. The rotation of the die causes that the feedstock layer is compressed as the spacing between die and roller decreases. At some point, the compressional force between die and roller exceeds the frictional resistance of the feedstock in the press channel, and the compressed layer of feedstock is pressed into the press channels.

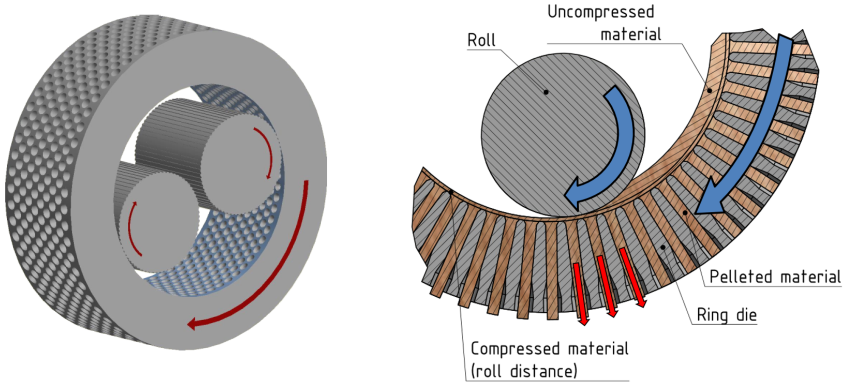

(a) Rotating ring die with two rollers.

(b) Cross-sectional view of a ring die and roller.

Figure 1.2: Ring die pellet press (figure from paper B [15]).

Pressing the feedstock layer into the press channels initiates motion of the feedstock in the channels, which is illustrated by the red arrows in figure 1.2b. The motion causes compressed cylinders of feedstock being extruded from the outside of the die, where a knife break the compressed feedstock into pellets. The pressure required for pressing the feedstock into the press channels is specified as the pelleting pressure. The pelleting pressure is challenging to measure directly in the pellet press, and not many studies have reported such measurements. However, a few studies have stated the pressure to be in the range 100-410 MPa [18,25]. Hence, the dies are produced of high strength alloys to resist deformations caused by the pelleting pressure,

causing that the cost price for one die can reach 10,000 €.

Based on experiences from the industry, the life time before replacement or renovation of the wear parts of pellet press are highly dependent on the process and type of feedstock. Dies used for wood pelleting can have a life time up to approximate 2500 hours, while productions with abrasive feedstocks as agricultural crops, that have higher contents of silicate, generally have shorter life times.

The design of the die is primarily focused on the design of the press channel itself, while the distribution and number of channels in the die rarely are used as active design parameters. For ring dies, press channels are typically distributed in hexagonal patterns. For industrial dies, the number of press channels is typically selected to equal 30-40% opening area of the total die area. The opening area is defined as the accumulated area of the press channels and is a tradeoff between die strength and increasing the number of press channels.

Figure 1.3 illustrates a cross-sectional drawing of a press channel, which consists of an active and inactive section. The active section is where the feedstock is in sliding contact with the die and consists of a conical inlet and a cylindrical channel. The inactive section has no direct effect on the pelleting process, other than adding strength to the die to resist it from breaking.

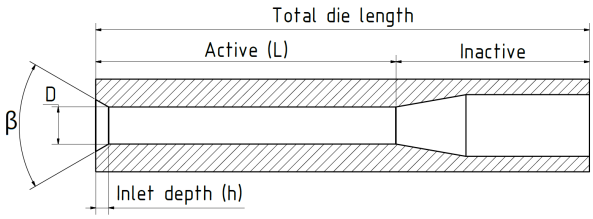

Figure 1.3: Cross-sectional view of a press channel (figure from paper B [15]).

The ratio of length and diameter, L/D, of the press channel's active part is a commonly used design parameter when designing the die. Increasing the L/D ratio increases the frictional resistance between feedstock and die, and thereby increases the pelleting pressure [26]. The typical press channel is between 6 and 8 mm in diameter with an L/D between 3-7 for wood and 7-12 for agricultural feedstock [15].

The conical inlet is specified by the angle, β, and depth, h. The inlet is where the feedstock layer is pressed from the die surface and into the press channel. The effect of the inlet design on the pelleting process is not well understood in the apparent literature, which is shown by the literature review in paper B. However, Nielsen et al. [25] showed via single pelleting tests that a significant part of the energy consumption is consumed in the

inlet section, when using an 8 mm channel with a typical inlet design of $\beta = 60^{\circ}$ and $h = 2.5$mm .

The die is the central part of the pellet press, and must be designed correctly to produce pellets with sufficient density and mechanical durability without using excess energy, which increases the OPEX of the production.

From the literature review of the pelleting process performed in paper B, the following points are highlighted:

- The L/D ratio of the die is likely the most commonly used design parameter of the die, while the effect of parameters such as die area, press channel inlet design, roller gap, and rotational die speed are rarely reported in papers of pelleting studies.
- A few studies have indicated that the press channel inlet has an effect on the pellet durability and energy consumption. However, the research has not resulted in correlations between the design and the process or pellet properties have been shown.
- Consideration of the feedstock's mechanical properties, such as stress relaxation, varying frictional coefficients, and changes in feedstock properties could improve the understanding of pelleting process, and improve existing calculation models for the pelleting pressure, which are discussed in chapter 2.

1.4 Outline of the Papers

The thesis is structured as an extended summary based on the contribution of five papers. The extended summary describes the background and motivation for the project and a summary of the papers. Figure 1.4 illustrates the chronology of the papers in this thesis, and the description of the papers as follows:

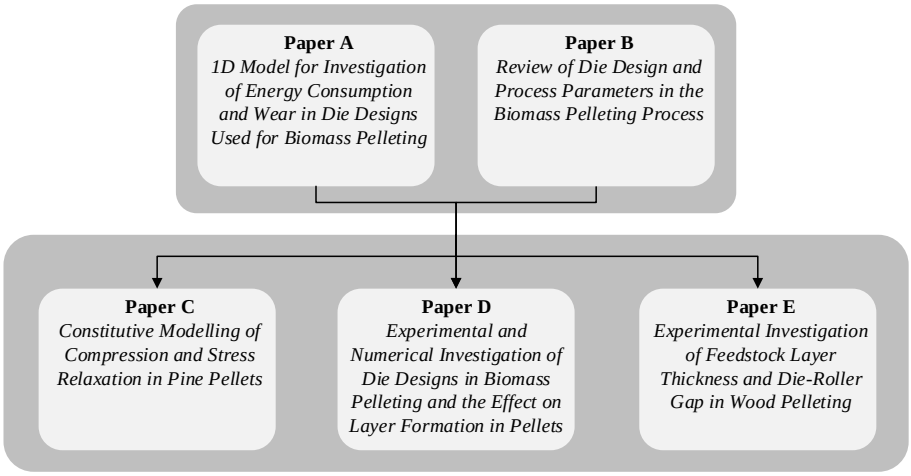

Figure 1.4: Chronology of the five papers in this thesis.

1D Model for Investigation of Energy Consumption and Wear in Die Designs Used for Biomass Pelleting

- This paper aims to improve the understanding of the physical processes in terms of die wall friction and feedstock compression in the press channel of the die. A 1D model of a press channel is set up, which is capable of simulating the pelleting pressure and energy consumption for compression and friction in press channels.

Review of Die Design and Process Parameters in the Biomass Pelleting Process

- This paper presents a literature review, and covers the effect of design- and process parameters in the pelleting process. In the paper, an overview d of designs and process settings used in previous pelleting studies is presente. Together with Paper A, this paper forms the basis for the following work in this project, where limitations of the 1D model and identified gaps in the current state-of-the-art, are used as topics for the papers C-E.

Constitutive Modelling of Compression and Stress Relaxation in Pine Pellets

- From the more simple constitutive model employed in the 1D model from paper A, a model that captures the viscoplastic properties of biomass fibers is presented. The model is a Maxwell representation of the Standard Linear Solid (SLS) model with non-linear elastic properties. The mechanical feedstock properties for six different particle size samples of spruce and three compression speeds were derived by fitting the model to experimental compression tests. The constitutive model and mechanical properties give new insight into the behavior of biomass particle compression and have utility for improving simulations of the pelleting process by capturing the stress relaxation effects of the feedstock.

Experimental and Numerical Investigation of Die Designs in Biomass Pelleting and the Effect on Layer Formation in Pellets

- The review in paper B showed that a minimal number of research studies had been dedicated to the design parameters of the press channel inlet and the effect on the pelleting process. However, the review also showed that the inlet tends to have a significant effect on the pelleting process, which also was found from the experimental and simulation results in paper A. This paper presents a Computational Fluid Dynamic (CFD) model that is capable of simulating the feedstock motion in the press channel inlet. Also, the paper presents an analysis of the feedstock layers shapes in the pellets, and shows a link between the press channel inlet and the mechanical durability of the pellets.

Experimental Investigation of Feedstock Layer Thickness and Die-Roller Gap in Wood Pelleting

- The results of paper A showed a significant difference between the experimental and simulated energy consumptions of the tested press channels. A reason for this is probably that the 1D model does not capture the transient effects of the start-stop motion in the press channel when subsequent feedstock layers are pressed into the channel. The literature review in paper B, also showed that a very limited research has been dedicated to studying the effects of the feedstock's start-stop motion, die speed, and roller gap size.

  This paper aims to show the effect of the start-stop motion, where experimental pelleting tests are carried out using a pilot-scale pellet press, which was set up for this study. By varying the feedstock mass flowrate and die speed, a range of different feedstock layers was tested. The study also includes tests with different die-roller gaps.

Chapter 2

Press Channel Analysis

In this chapter, a brief review of equations for calculation of pelleting pressure is given. The review is followed by a presentation of a 1D model for calculating the pelleting pressure and the energy consumption for pelleting, which is based on an analysis of the governing forces in the die press channels. Finally, model calculations are presented together with an evaluation of the model capability and limits.

2.1 Pelleting Pressure

As discussed in the thesis introduction, the pellet press die shall facilitate the production of pellets that have a quality according to the requirements, without using excessive energy and reducing the production capacity of the pellet press.

The press channel design is directly correlated to the pelleting pressure [26], which affects the degree of compression of the feedstock and the power consumption required for the pellet production [12]. When pressing the feedstock through the press channels, the pelleting force equals the accumulated resisting forces of pressing feedstock into the press channel and the friction between the feedstock and the wall of the press channel.

Figure 2.1 illustrates the forces in the press channel, where F_r is a radial force in the feedstock, F_μ is the friction force between the feedstock and the wall of the press channel, and F_p is the pelleting force. As illustrated in figure 2.1, the friction force acts in the opposite direction to the pelleting force. The radial force is the normal force acting on the wall due to the radial expansion of the feedstock, which is constrained by the die wall.

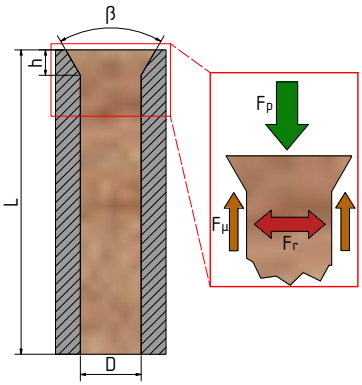

Figure 2.1: Cross-sectional drawing of the active section of the press channel, and an illustration of the forces that acts in the channel, where F_p is the pelleting force, F_r is the radial force, F_μ is the friction force.

Pelleting Pressure Calculation

Calculation of the pelleting pressure for a specific press channel design, can help to identify if the pressure is within the typical range of pelleting pressures, and be used for stress calculations of the die [27]. Previous studies have used formulas for calculating the pelleting pressure, where the effect of feedstock properties and geometrical press channel parameters are included. Equation 2.1 by Holm et al. [26] and equation 2.2 by Crawford et al. [12] are examples of pelleting pressure equations. In paper B, a table with more equations and a thorough description of them can be found.

$$P_p = \frac{P_{No}}{\nu} \cdot \left(e^{4 \cdot \mu_w \cdot \nu \cdot L/D} - 1 \right) \tag{2.1}$$

$$P_p = P_c \cdot e^{4 \cdot \mu_w \cdot k_r \cdot L/D} \tag{2.2}$$

In equation 2.1, P_p is the pelleting pressure, P_{No} is a prestressing pressure, ν is the Poisson's ratio of the feedstock, and μ_w is the coefficient of friction between the feedstock and die wall. In equation 2.2, P_c is a compression pressure, and k_r is the axial to radial stress ratio of the feedstock.

Equation 2.1 by Holm et al. [26] is based on an elastic-plastic stress-strain model for calculating the radial force in the press channel as a function of the applied pelleting pressure. The radial prestressing pressure, P_{No}, is a constant pressure which is added to the elastic response of the applied forces. In their study, Holm et al. [26] assumed the biomass fibers to be oriented normal to the die wall, which affects the value of Poisson's ratio. The effect of fiber orientation is caused by the anisotropic properties of biomass, which experimentally is shown to affect the pelleting process [28].

Equation 2.2 by Crawford et al. [12] is very similar to the equation by Holm et al. [26]. However, Crawford et al. [12] only utilizes an elastic stress-strain model for calculating the radial force, and introduces an compression pressure, P_c, which is the pressure required for compressing the feedstock to a desired density. Crawford et al. [12] showed a correlation between the electrical power consumption of the pellet press and the calculated pelleting pressure. In addition, Crawford et al. [12] found that the friction account for 60-80% of the energy consumption, while the remaining part of the energy is used for compression.

By evaluating the equations for the pelleting pressure in equation 2.1, 2.2, and the equation framework [26, 29–32] that is shown in paper B, there are several similarities, where properties as Poisson's ratio, or axial to radial stress ratio of the feedstock, the coefficient of friction, and the press channel L/D, all recur in the equations. The equations are limited to calculation of the pelleting pressure or force for a pure cylindrical press channel, except equation 2.3 by Osobov [29], which is based on the calculation of a conical briquetting channel that is comparable to the inlet section of the press channel. However, instead of calculating the required pelleting pressure, equation 2.3 by Osobov [29] uses the pelleting pressure as input and calculates the local pressure in the press channel, P_x, where x is the distance from the top of the inlet.

$$\begin{aligned} P_x &= P_p \cdot \left(\frac{D - 2 \cdot x \cdot tan(\beta)}{D} \right)^n \\ n &= \frac{2k}{tan(\beta)} \cdot (sin(\beta) + \mu \cdot cos(\beta)) \end{aligned} \tag{2.3}$$

The pressure equations for a cylindrical press channel demonstrates a positive exponential correlation between the pelleting pressure and the L/D ratio of the press channel. The same exponential correlation has been shown in single pelleting studies [16, 33, 34].

2.2 1D Press Channel Model

As mentioned, the presented equations for calculating the pelleting pressure are restricted to calculation of pure cylindrical press channels. Thus, a 1D model that accounts for the inlet design parameters, β and h, for calculation of the pelleting pressure is set up. Also, the model calculates the feedstock density and energy required for the feedstock compression and friction.

The assumptions for the model are as follows:

- The model is based on a steady-state model of the pelleting process, with a constant mass flow rate through the press channel.

- No transverse velocity gradients of the feedstock in the press channel, in other words, the feedstock moves as a plug.
- Feedstock properties are taken from properties for solid wood, where the orientation of the feedstock fibers are transverse the press channel.
- Isothermal conditions applies, and thereby effects of frictional heating of the feedstock in the press channel are neglected.

The calculation of the pelleting pressure is based on the force balance in equation 2.4, where the force of the pelleting pressure, F_p in figure 2.1, equals the friction force, F_μ, which is a function of the radial force, F_r.

$$F_p = F_\mu + F_0 \tag{2.4}$$

In equation 2.4, F_0 is introduced as an imaginary outlet force that acts in the opposite direction F_p. F_0 is used when discretizing the press channel, which is described in section 2.2.

Calculation of F_r is performed using equation 2.5. Equation 2.5 is based on the formulation by Holm et at. [26], where the radial force is derived from two terms; elastic and plastic, where the elastic force, based on Hook's law, is a function of the pelleting force in the channel, and the plastic term is a constant stress.

$$F_r = \underbrace{\frac{A_r}{A_a} \cdot \nu \cdot F_p}_{\text{Elastic}} + \underbrace{P_{No} \cdot A_r}_{\text{Plastic}} \tag{2.5}$$

In equation 2.5, A_r is the area of the press channel wall on which the radial force acts, A_a is the cross-sectional area of the press channel on which the pelleting force acts, ν is Poisson's ratio, and P_{No} is the constant stress in the plastic term.

For a cylindrical channel, F_μ is calculated as the product of F_r and μ_w. However, in the conical part, F_r is split into two components, which are illustrated in figure 2.2, with the first component, F_{rn}, acting normal to the die wall, and the second component, F_{rp}, acting parallel to the wall.

Based in the illustration in figure 2.2, F_μ is calculated from equation 2.6.

$$F_\mu = \cos(\beta/2) \cdot \left(F_{rn} \cdot \mu_w + F_{rp}\right) \tag{2.6}$$

For the cylindrical channel with $\beta = 0^\circ$, equation 2.6 reduces to the product of F_r and μ_w.

From the force balance in equation 2.4, the expression for F_p is set up in equation 2.7 by combining equation 2.5 and 2.6.

$$F_p = \frac{F_0 + \cos(\beta/2) \cdot P_{No} \cdot A_r \cdot (\cos(\beta/2) \cdot \mu_w + \sin(\beta/2))}{1 - \cos(\beta/2) \cdot \frac{A_r}{A_a} \cdot \nu \cdot (\cos(\beta/2) \cdot \mu_w + \sin(\beta/2))} \tag{2.7}$$

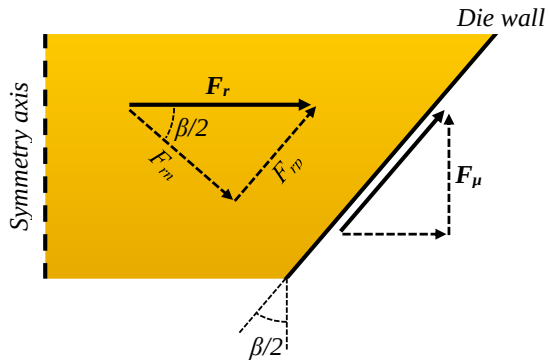

Figure 2.2: Illustration of the force components of F_r and F_μ in the conical inlet of the press channel (figure from paper A [35]).

Energy Consumption in the Press Channel

The 1D model is set up to calculate the frictional and compressional energy that is consumed in the press channel. The energy is calculated as outlined in figure 2.3.

Frictional Work

The frictional power dissipation, $\dot{W}_\mu$, is calculated via equation 2.8

$$\dot{W}_\mu = F_\mu \cdot \frac{\dot{m}}{\rho \cdot A_a} \tag{2.8}$$

In equation 2.8, $\dot{m}$ is the feedstock mass flow rate, and ρ is the feedstock density. $\dot{W}_\mu$ is converted to a mass-specific energy consumption, w_μ, by using equation 2.9.

$$w_\mu = \frac{\dot{W}_\mu}{\dot{m}} \tag{2.9}$$

Compressional Work

The compressional work consumed for compressing the feedstock is calculated as the definite integral of compression pressure over the change in mass-specific volume during compression of the feedstock. The compressional work is illustrated as the blue-colored area in figure 2.4, where equation 2.10 is the expression of pelleting pressure as a function of the specific volume for the feedstock, v. The function in equation 2.10 is derived from a power function that was fitted to experimental compression tests. Further information about the experimental compression test and the power function

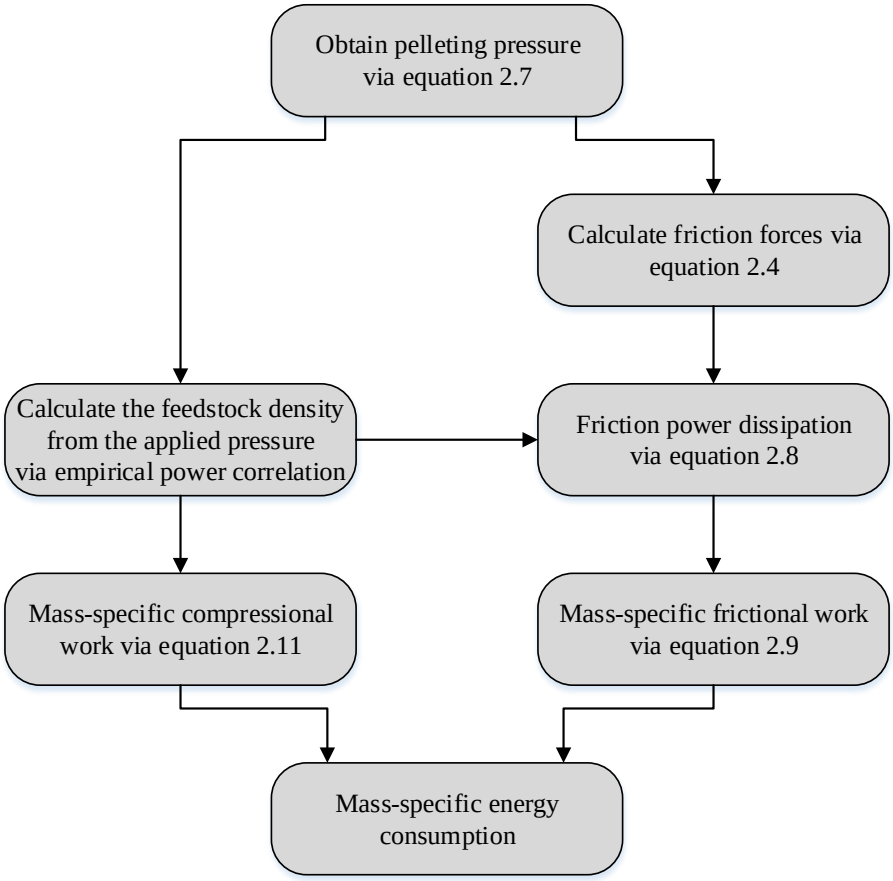

Figure 2.3: Outline of the algorithm for the energy calculation from friction and feedstock compression.

is described in paper A.

$$P_p(v) = \left(\frac{1}{k_1 \cdot v} - \frac{k_3}{k_1} \right)^{\frac{1}{k_2}} \tag{2.10}$$

In equation 2.10, k_{1-3} are empirical coefficients obtained by fitting the power function to the experimental compression data. The coefficients values are: $k_1 = 318.892$, $k_2 = 0.276$, and $k_3 = 12.634$.

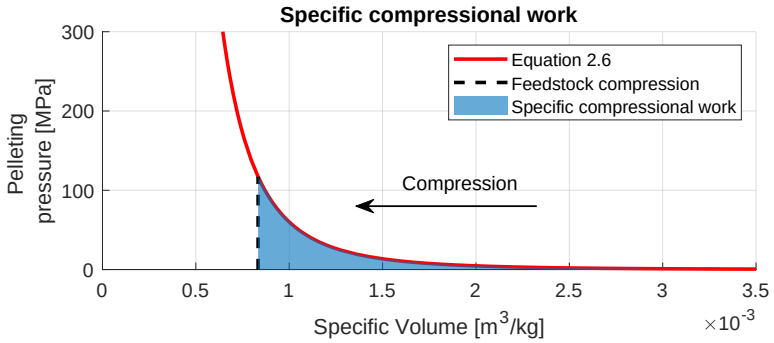

Figure 2.4: Plot of the pelleting pressure as a function of the specific volume of the feedstock, where the blue colored area is the mass-specific compression energy (figure from paper A [35]).

The mass-specific energy consumed for compression of the feedstock, w_c, is calculated via the integral in equation 2.11.

$$w_c = \int_{v_1}^{v_2} P_p(v)\, dv \tag{2.11}$$

In equation 2.11, v_1 and v_2 are the initial and final specific volume of the feedstock.

Press Channel Discretization

To calculate F_p in equation 2.7, the press channel is discretized into N-number of even spaced elements, where each element represents a disk of the press channel. Figure 2.5 illustrates a discretized press channel, with the boundary condition that $F_o(n = N)$ equals zero. $F_p(n = 1)$is the overall pelleting force.

The elements in the press channel are coupled by the expression in equation 2.12.

$$F_p(n) = F_0(n - 1) \tag{2.12}$$

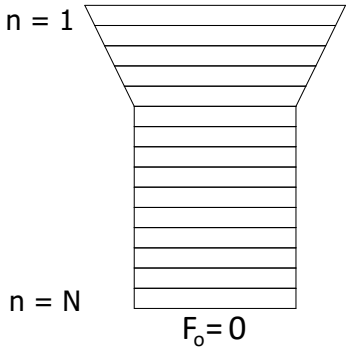

Figure 2.5: Discretized press channel with N-number of elements, and the boundary condition, $F_0 = 0$.

Figure 2.6 shows a plot of the calculated pelleting pressure for different discretization levels of a pure cylindrical press channel, with element numbers between 10 and 13,000. The pelleting pressure is calculated as F_p divided by A_a. The 1D model results are compared to the pelleting pressure calculated using equation 2.1 by Holm et al. [26]. Figure 2.6 shows that by increasing the number of elements in the 1D model, the pressure approaches the analytical solution from equation 2.1. Figure 2.6 also shows, that the 1D model becomes more or less independent of the discretization with approximate 1000 elements, and adding more elements to the model does not affect the pelleting pressure calculation considerably.

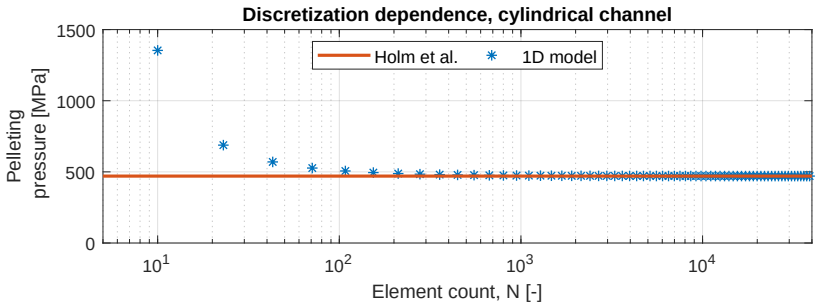

Figure 2.6: Comparison between the 1D model with different numbers of elements and the equation by Holm et al. [26]. The pressure is calculated for a 50 mm press channel with a diameter of 6 mm.

2.3 Model Results

The model performance was evaluated by comparing simulated and experimental pelleting pressures. The experimental pelleting pressures were measured from single pelleting tests with spruce at a temperature of 100 °C. Four dies with different inlet designs were tested. The simulations were performed with the properties and settings listed in table 2.1, where the friction coefficient is fitted such that the experimental and simulation result of die no. 1 matches, since no measurements of the friction coefficient is performed. The fitted friction coefficient is within the typical range of friction coefficients for wood [36]. More information about the single pelleting tests, feedstock properties, and model settings are reported in paper A.

Table 2.1: Feedstock properties and model settings.

$\dot{m}$	ν	P_{No}	μ	N	L	D
0.35 g/s	0.255	2.74 MPa	0.463	4000	50 mm	6 mm

The results of simulations and experiments are listed in table 2.2, and shown in figure 2.7 where the simulated and experimental pelleting forces are compared. The error bars in figure 2.7 indicate the standard deviation of the final four layer presses of the experimental measurements for each die. The standard deviations are shown in parentheses in table 2.2.

The measuring uncertainty of the force transducer used in the experiments is 0.5% of the reading value, and therefore the uncertainty is between ±60-96 N for the four dies.

The experimental pelleting forces in table 2.2 are measured as the highest recorded force for pressing a layer into the die, and the energy consumption is calculated by numerically integrating the force vs. displacement of the pressing piston in the single pelleting setup.

Table 2.2: Experimental and simulation results from the single pelleting tests from paper A, where the numbers in parentheses indicate the standard deviations.

Die			**Simulation**			**Experiment**	
No.	β [°]	h [mm]	Pelleting force [N]	Total energy [J/g]	Compression energy vs. friction energy [% vs. %]	Pelleting force [N]	Total energy [J/g]
1	0	0.0	13,236	366.5	27.3 vs. 72.7	13,220 (±212)	149.1 (±5.0)
2	40	4.1	16,905	412.8	21.1 vs. 78.9	19,165 (±362)	187.4 (±5.8)
3	80	1.8	16,102	420.7	23.7 vs. 76.3	16,326 (±1,142)	171.4 (±6.3)
4	120	1.0	14,416	398.5	25.1 vs. 74.9	16,195 (±340)	157.4 (±3.8)

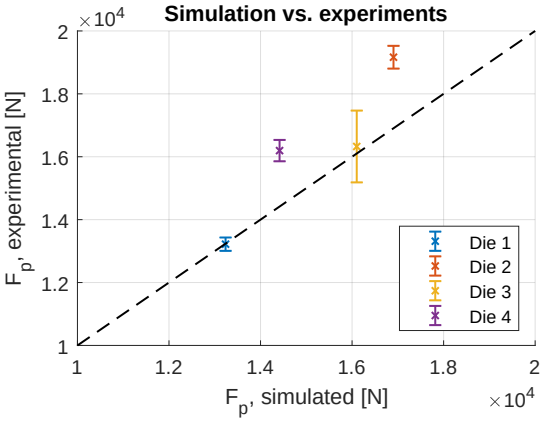

Figure 2.7: Plotted results of the simulated and experimental pelleting forces from paper A.

The results in figure 2.7 and table 2.2 show that the model, to some extend, is capable of simulating the pelleting force for the four press channels. However, the simulated pelleting force is lower than the experimental force for die no. 2 and no. 4.

Besides calculating the pelleting force, the model can simulate the pressure and feedstock density inside the press channel. As an example, figure 2.8 shows contour plots of the simulated pressure and feedstock density in press channel no. 3 from the tests. The pressure is calculated as F_p divided by the area, A_a, of the model elements. The feedstock compression is assumed to be irreversible, meaning that when the pressure is decreases, the density does not decrease.

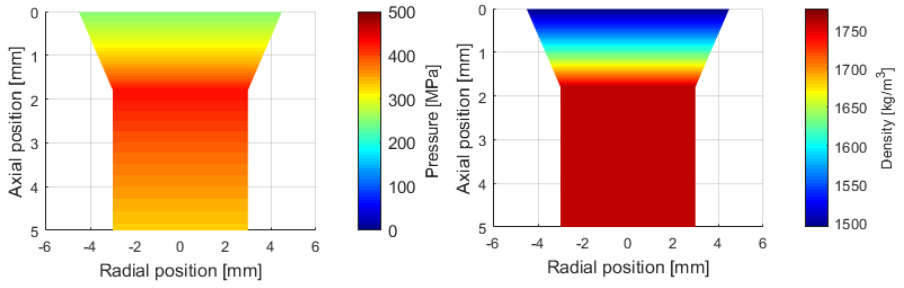

(a) Pressure

(b) Feedstock density.

Figure 2.8: Contour plots of the simulated pressure and feedstock density in the upper part of press channel no. 3.

Figure 2.8a shows that the pressure peaks at the transition between the inlet and the cylindrical part of the press channel. The simulated density in

figure 2.8b shows that the compression occur in the inlet of the press channel, and not in the cylindrical channel. The simulated pellet density of approximate 1750 kg/m^3 for die no. 3 is above the normal level for reported pellet densities which is 1100-1300 kg/m^3 [25,37], and is also above the maximum obtainable density of 1420-1500 kg/m^3 for compressed biomass [38,39]. The reason for the high density is caused by an extrapolation of the empirical power function, which is fitted for pelleting pressures below 250 MPa, while the simulation shows a peak pressure above 400 MPa. Therefore, the power function of the density should be evaluated further, where experimental data from higher pressures should be collected.

Press Channel Wear

The high pressure that acts in the press channel causes abrasive wear on the die. Figure 2.9 shows measurements from a 3D scan of a worn 8 mm ring die [40]. Figure 2.9a and 2.9b show that the inlet of the press channel is exposed to a significant degree of wear, while the lower part of the channel almost is intact.

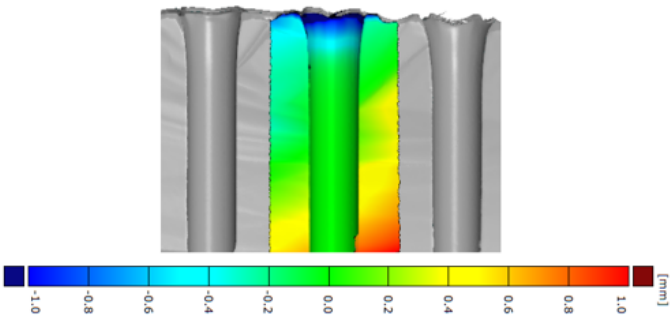

(a) Contour plot of the worn die, where the color indicates the geometrical difference between the worn and original die.

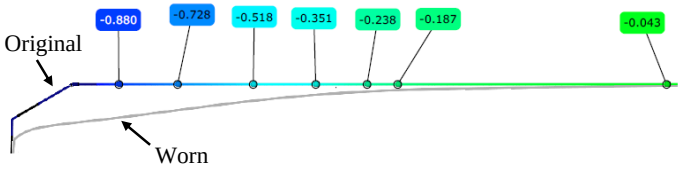

(b) Illustration of the upper 15 mm press channel wall of the original and worn die, where the numbers indicate the distance between the two shapes. The inlet of the press channel is on the left side.

Figure 2.9: 3D scan measurements of a worn die with 8 mm press channels (figure from Andritz report [40]).

Comparing the 3D scan measurements and the simulated pressure contours in figure 2.8a, shows that the wear is concentrated in the region where

the highest pressure in the press channel is observed.

Model Limitations and Future Work

The plot in figure 2.7 shows a deviation between the 1D model and the experimental pelleting pressures for die no. 2 and no. 4. A reason to the difference may be explained by the model not accounting for internal friction in the feedstock, when it is deformed or folded in the conical inlet. According to results from Nielsen et al. [25], the press channel inlet has a significant impact on the pelleting energy. The 1D model accounts for the friction between the feedstock and press channel wall, but the assumption of no transverse velocity gradients in the press channel, neglects the viscous resistance from internal folding or layer deformation of the feedstock, which may influence the 1D model performance. The effect of the press channel inlet on the feedstock folding or layer deformation is the scope of paper D and is described and discussed in chapter 4 of this thesis.

The results in table 2.2 show that the energy consumption for the experimental results is in the range 149.1-187.4 J/g, corresponding to 37.6-47.2 kWh/t, which are comparable to normal energy consumptions for industrial-scale pellet presses [21–24]. However, the simulated energy consumptions are 2.2-2.5 times higher than the energy consumption of the experimental results. This difference may be caused by the assumption of simulating the pelleting process a steady-state, where the pelleting pressure is assumed to be constant. Thus, the 1D model does not account for the frictional effects of the feedstock's start-stop motion in the press channel, which occurs in pellet press and in the performed single pelleting tests. In pellet presses, the friction constantly switches between a static and kinetic level when feedstock layers are pressed into the channels, which causes a dynamic pelleting pressure. The start-stop of the feedstock in the press channel is the topic of chapter 5, where the effects will be analyzed.

In addition to inlet and start-stop effects, the use of constant feedstock properties, and neglecting frictional heating are likely to affect the model accuracy. At elevated temperatures, the extractives in the feedstock, as oil and wax, migrate to the surface of the compressed feedstock, which may reduce the friction [16]. Another effect of increased temperature is the transition temperature of the lignin, at which the polymer stiffness decreases when shifting from its glassy phase towards the rubbery phase [41]. The lignin transition temperature for biomass ranges between 50-140 °C [42–45], and depends on the feedstock specie and moisture content [37, 46]. By reaching pelleting temperatures above the lignin transition temperature, the inter-particle contact area is likely increased from softened lignin filling the gaps in the compressed feedstock [47, 48], which enables stronger bonding between the particles [49, 50]. Solving the die and feedstock temperature, and applying

the mechanical properties, ν and μ_w, as functions of temperature, could improve the model performance. Also, simulation of the feedstock temperature can show if and when the lignin or other lignocellulosic components are softened during the pelleting process. Thereby, the simulation could be used for analyzing if the feedstock temperature is in the range that may improve the pellet durability due to softened lignin.

Chapter 3

Constitutive Modelling of Pelleting Feedstock

In this chapter, the compressional characteristics of biomass grinds are investigated. A brief review is given on existing constitutive models for simulating the feedstock stress and strain during compression and stress relaxation. The review is followed by a presentation of a constitutive model for deriving rheological properties of a feedstock and the correlation of these to relevant pelleting properties as energy consumption and pellet durability.

3.1 Biomass Compression

The compression of feedstock is essential to the pelleting process, as the bulk density of wood pellets shall be minimum 600 kg/m^3, according to the ISO 17225-2:2014 [10]. The densification of feedstock between the pellet press die and roller depends on the level of compression, or strain, of the feedstock, when reaching the stress level of the pelleting pressure. By knowing the stress-strain relation of the feedstock it is therefore possible to calculate the required level of pelleting pressure to obtain a given density of the compressed feedstock. The mechanical behavior for biomass feedstock is characterized by viscoplastic properties [51]. Figure 3.1 illustrates a force vs. time recording from a uniaxial compression of spruce, and the corresponding piston displacement that compresses the spruce.

The plot in figure 3.1 is split into two phases; compression and stress relaxation. The compression phase is marked by the blue-shaded area, where the applied force increases nonlinearly. The nonlinearity is caused by changes in the mechanical behavior of the compact, as different physical mechanisms prevail during the compression [52, 53]. Generally, the compression can be

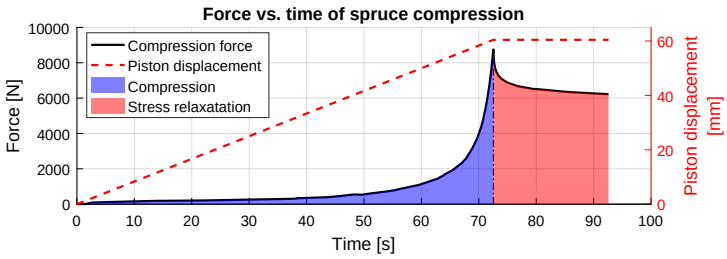

Figure 3.1: Plot of force and piston measurements during compression of a spruce sample, showing the characteristic viscoplastic stress relaxation of the compressed biomass (data from compression test for paper A [35]).

split into two phases:

1. The initial compression phase is dominated by rearrangement of the particles, where a high porosity from air voids is present in the compact. Faborode et al. [54] defined the end of this phase using a critical density, which they suggested to be at the peak of the Cauchy number, which is the ratio of the inertia and elastic forces of the compact. In their study, Faborode et al. [54] reported a critical density of 411 kg/m^3, which was obtained at a compression pressure at approximately 4 MPa. Kaliyan et al. [55] analyzed the force gradients to define the end of the initial compression phase, which they reported to occur at 1.5 MPa. Compared to figure 3.1, 1.5-4 MPa is equal to forces of approximately 100-300 N. Thereby, the initial compression phase is more or less insignificant to the pelleting process and the energy required to compress feedstock to densities of pellets.

2. In the second phase, the compression of the particles begins as the particle contact increases, and the porosity decreases. When the air is expelled from the compact, elastic forces become dominant in the compact [54].

After the compression phase, the stress relaxation appears, which is marked by the red-shaded area in figure 3.1. As indicated by the piston displacement plot in figure 3.1, the compressed sample is exposed to a static strain, and the apparent forces in the feedstock are measured from the piston. The physical mechanisms of the stress relaxation are governed by a plastic flow of the compressed biomass particles [56]. The decreasing stress is caused by the compressed particles rearranging as the elastic energy of the particles is converted to plastic deformations. Under static conditions, the residual stress of the compacted biomass approximates an asymptotic level, where no further relaxation occurs [57].

In the pellet press die, the stress relaxation occurs while the compressed

feedstock is pressed through the press channels. When the feedstock is released from the die, residual stresses in the feedstock are transformed into axial and radial expansions of the pellet [58, 59]. High residual stresses of the compressed feedstock, causes more expansion, which has been found to decrease the durability of the pellets [60]. Peleg [57] defined the asymptotic modulus from stress relaxation curves of compressed biomass samples and found that samples with high asymptotic modulus were more rigid and could sustain higher residual stresses.

Constitutive Models

The constitutive modeling approach is based on a theoretical approach, where systems of rheological elements are set up to simulate materials mechanical stress-strain responses. Elements as springs and Coulomb friction are applied to describe pure elastic and plastic behavior. Time-dependent responses of viscoelastic and -plastic materials are modeled using dashpot elements, where the stress is a function of the strain rate. Using constitutive models, ease the interpretation of the model parameters to the feedstocks mechanical properties.

In figure 3.2, schematic drawings of four general constitutive models are shown. More models and a detailed description of them are found in paper C.

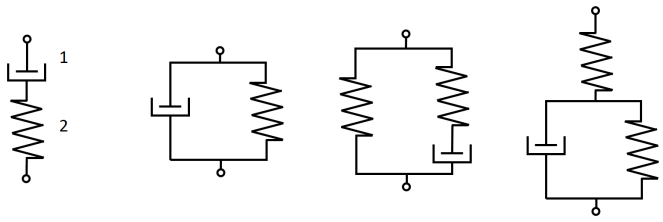

(a) Maxwell **(b)** Kelvin-Voigt **(c)** SLS, Maxwell **(d)** SLS, Kelvin-Voigt

Figure 3.2: Representation of constitutive models presented in previous compression studies. Symbol explanation: spring[1], dashpot[2] (figure from paper C [61]).

The capability of the four models in figure 3.2 to simulate compression and stress relaxation responses is evaluated by the simulations in figure 3.3, where the time up to t_1 is the compression phase, and after t_1 is the stress relaxation phase.

Evaluated from the plots in figure 3.3, the Standard Linear Solid (SLS) Maxwell and SLS Kelvin-Voigt models are capable of simulating a stress relaxation that is similar to the experimental compression data in figure 3.1, where the stress gradually decreases towards an asymptotic level. The

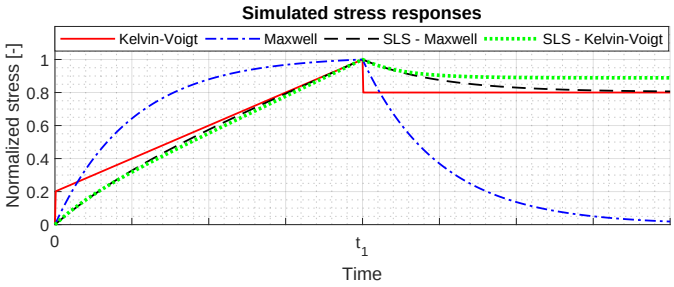

Figure 3.3: Simulated responses from the constitutive models in figure 3.2 (figure from paper C [61]).

Maxwell model is not capable of simulating the asymptotic stress level of the relaxed feedstock, due to the serial connection of the spring and dashpot. Hence, the elastic energy stored in the spring is dissipated to the viscous deformation of the dashpot.

The Kelvin-Voigt model fails in simulating the gradual stress decrease of the stress relaxation, since all the elastic energy of the spring is maintained under static conditions, and no viscous dissipation occurs.

The simulated responses in figure 3.3 also show that the four models are not capable of modeling the nonlinear behavior of the compression phase as observed in figure 3.1.

Nonlinear Mechanical Properties

Different approaches for modeling the nonlinearity of the stress-strain during biomass compression has been proposed. Peleg [62], Faborode et al. [63], and Kaliyan et al. [55] applied strain-hardening springs to their models, where the spring is modeled with a linear and nonlinear term. Molari et al. [64] used a nonlinear spring formulation based on conical springs to model the compression of straw bales. The need for applying elements with nonlinear characteristics, such as strain hardening springs, is due to the mechanical properties of the bulk feedstock, such as the density, which is dependent on the mechanical stress. Carone et al. [65] found a positive exponential correlation between Young's modulus of pellets and the pellet density like they also found it to be dependent on the feedstock particle size, temperature, and moisture content.

3.2 Constitutive Model for Compression and Stress Relaxation

A constitutive model based on the SLS Maxwell model that is capable of simulating compression and stress relaxation of biomass is set up. The SLS Maxwell model is chosen due to its low complexity with three elements. To model changes in the mechanical behavior of the feedstock during compression, nonlinear strain-hardening properties are added to the model's two springs. The assumptions for the model are as follows:

- The feedstock behaves as a continuum.
- The friction between die and feedstock is neglected, and thereby, there are no pressure or density variations inside the compressed sample.
- The initial compression phase is neglected [55].

Figure 3.4 shows a detailed mechanical representation of the SLS Maxwell model, which is split into two parallel systems. In figure 3.4, system 1 is

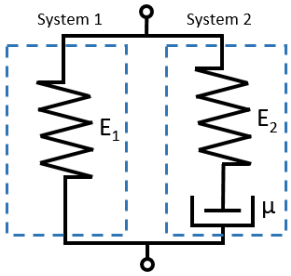

Figure 3.4: Detailed mechanical representation of the SLS Maxwell model (figure from paper C [61]).

based on a single spring, with the spring modulus E_1. System 2 is a Maxwell system, with a serial connection of a spring, with the spring modulus E_2, and a dashpot with the viscosity, μ. From the SLS Maxwell configuration, the asymptotic value of the residual stress can be interpreted as the stress in system 1, as system 2 eventually relaxes to zero stress. The constrains of SLS Maxwell model in figure 3.4 are expressed in equation 3.1, where σ is the total stress, σ_1 and σ_2 are the system stresses, ϵ is the total strain, and ϵ_1 and ϵ_2 are the system strains.

$$\epsilon = \epsilon_1 = \epsilon_2 \tag{3.1a}$$

$$\sigma = \sigma_1 + \sigma_2 \tag{3.1b}$$

The model stress is calculated via the expression in equation 3.2, which is derived in paper C by using a numerical approach with a temporal discretization of the compression.

$$\sigma(t+\Delta t) = \underbrace{E_1 \cdot \epsilon_1(t+\Delta t)}_{\text{System 1 stress}} + \underbrace{E_2 \cdot \frac{\epsilon(t+\Delta t) - (\epsilon(t) - \epsilon_{s2}(t))}{1 + \frac{E_2 \cdot \Delta t}{\mu}}}_{\text{System 2 stress}} \tag{3.2}$$

Equation 3.2 is based on a temporal discretization, Δt, where t is the time and ϵ_{s2} is the strain of the spring in system 2.

The spring modulus, E_1 and E_2, in the SLS Maxwell model are modeled using a pseudo spring porosity, which is based on a solid ratio vs. void ratio of the spring. The nonlinear spring modulus are calculated via equation 3.3c, which is derived by combining equation 3.3a and 3.3b.

$$E = x \cdot \frac{\phi_s}{\phi_v}, \quad \phi_v > 0 \tag{3.3a}$$

$$\phi_s = \frac{\rho_b}{\rho_s}, \ \ \phi_v = 1 - \frac{\rho_b}{\rho_s} \tag{3.3b}$$

$$E = x \cdot \frac{\rho_b}{\rho_s - \rho_b}, \quad \rho_b < \rho_s \tag{3.3c}$$

In equation 3.3, x is a spring coefficient, ϕ_v is the void ratio of the spring, ϕ_s is the solid ratio of the spring, ρ_b is the bulk spring density, and ρ_s is the true density of the solid spring. The bulk density of the feedstock during compression is inserted as ρ_b in equation 3.3c, and ρ_s is a constant fitted to each spring. The limiting condition for the expression in equation 3.3c, where ρ_b approaches the value of ρ_s, may be interpreted as the condition where the porosity of the compact goes toward zero, causing the spring modulus to approach infinity.

3.3 Results of Experimental Compression Tests

The performance of the SLS Maxwell model is evaluated by fitting the model fitted to experimental compression data of six spruce samples with different particle sizes. Figure 3.5 shows images of the five sieved spruce samples used for the experimental single pelleting tests, where the particle size ranges from 0.25-2.8 mm. The sixth sample is unsieved, and therefore has particle sizes ranging from 0-2.8 mm. The particle size samples are tested at three different compression speeds; 1, 5, and 10 mm/min, and each test combination of compression speed and particle size are repeated four times resulting in a total of 72 pellets produced.

(a) 0.25-0.5 mm **(b)** 0.5-0.8 mm **(c)** 0.8-1 mm **(d)** 1-1.4 mm **(e)** 2-2.8 mm

Figure 3.5: Sieved pine samples used for single pelleting tests (figure from paper C [61]).

The compression data were recorded from single pelleting tests, where pellets of feedstock samples were produced in two steps; first, the sample was compressed and after that pressed, or extruded, out of the die. Figure 3.6 illustrates a cross-sectional drawing of the single pelleting setup, where figure 3.6a shows the uncompressed feedstock, figure 3.6b shows the compressed feedstock, and figure 3.6c shows the extrusion of the pellet.

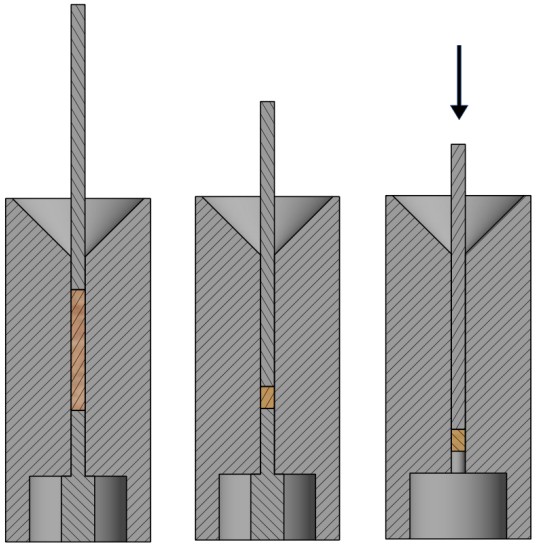

(a) Uncompressed **(b)** Compressed **(c)** Extrusion

Figure 3.6: The closed-end die setup used for the feedstock compression tests (figure from paper C [61]).

The compression and extrusion data were used for calculating the energy consumption of the process, and also, the durability was measured of the pellets produced from the different particle size samples. The die was heated to 90 °C, and the moisture content of the spruce was 14 % on dry basis.

The experimental results of compression energy, extrusion energy, and pellet durability are shown in figure 3.7, where the error bars represent the

standard deviation of the four repetitions for each combination of particle size and compression speed

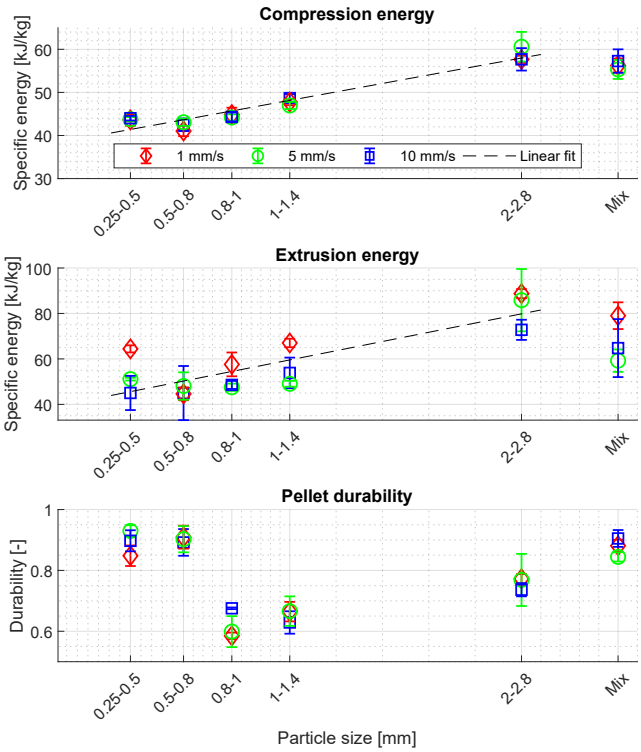

Figure 3.7: Experimental results of the specific compression energy, specific extrusion energy, total energy, and pellet durability (figure from paper C [61]).

In figure 3.7, the tendencies for the compression and extrusion energy are similar, where the energy is positively correlated with the particle size, while there is no significant effect of the compression speed. For the durability, the highest durability is produced of the two samples with the smallest particle sizes and the sample with mixed particle sizes. Further description of the experiments and information about the measurements are presented in paper C.

3.4 Simulation Results

The three constants of the SLS Maxwell model, x_1, x_2, μ are fitted to each of the 72 experimental data set, while $\rho_{s1} = 1206\ \mathrm{kg/m^3}$ and $\rho_{s2} = 1417\ \mathrm{kg/m^3}$ are based on a best fit to all 72 tests, and are kept constant. Figure 3.8 shows two plots where the simulated and experimental stress response for

the mixed particle size sample is shown for the three different compression speeds.

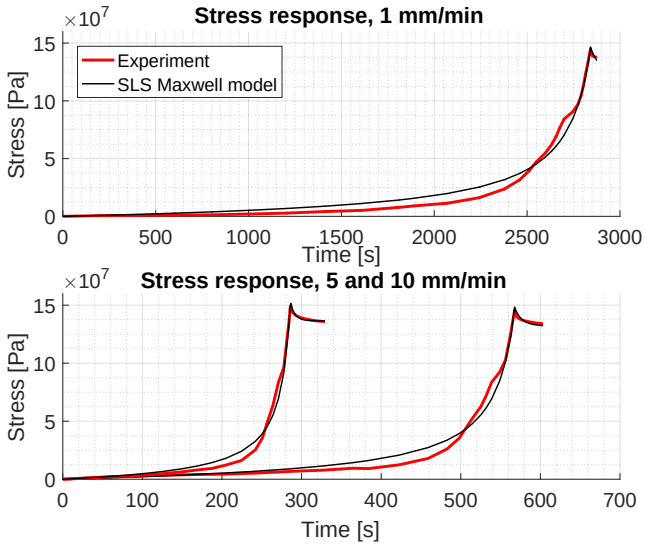

Figure 3.8: Experimental and simulated stress responses for the three compression speeds with the mixed particle size sample (figure from paper C [61]).

Generally, the simulated responses in figure 3.8 captures the compression and stress relaxation. The most considerable deviations between the experimental and simulated stresses are observed in the low-stress regions (<50 MPa), while the high stresses are matching well.

Figure 3.9 shows a plot of the simulated strain of the three model elements during a compression test. The strain of spring 1 increases linearly during the compression and is constant when the compression is stopped. For spring two, the strain increases and peaks after approximately 175 s whereafter it decreases, and the dashpot dissipates the elastic energy of the spring. The strain of the dashpot shows that a significant part of the damping, or stress relaxation, occurs during the compression phase, and only a small amount of energy is stored in spring two when the compression is stopped.

Mechanical Feedstock Properties

The fitted spring and damper coefficients from the model fits are plotted in figure 3.10, where the error bars represent the standard deviation of four replicates for each test combination, and the dotted lines are linear fits of the average element coefficients.

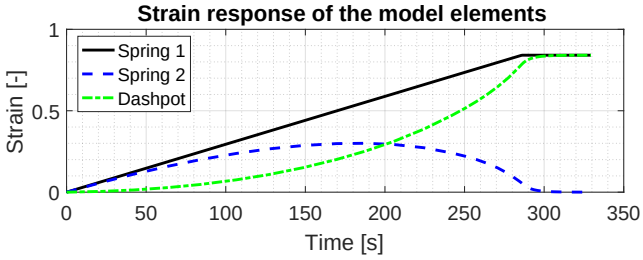

Figure 3.9: Simulated strain of the model elements during compression of the mixed particle size sample at a compression speed of 10 mm/min (figure from paper C [61]).

Spring 1

The coefficients of spring one in figure 3.10, shows that x_1 is more or less independent of particle size and compression speed for the 5 and 10 mm/min data. The x_1 coefficient for the 1 mm/min tests are slightly lower than the two other compression speeds and is negatively correlated to the feedstock particle size. As mentioned in section 3.2, the stress in spring one can be interpreted as the asymptotic value of the stress relaxation. Thus, the independence of particle size and compression speed for the 5 and 10 mm/min data might be explained by the pellets having reached a low porosity, and therefore the feedstock is homogenous, and its mechanical properties reassemble the properties of the solid feedstock. The lower x_1 coefficients of the 1 mm/min test might be explained by drying effects of the feedstock, due to a long retention time in the die compared to the 5 and 10 mm/min tests, since the elastic properties of biomass depend on the feedstock moisture content [36]. The drying effects were observed by an increased mass-loss of the pellets produced at 1 mm/min in the experimental test, which is described in paper C.

Spring 2

The coefficients of x_2 in figure 3.10 are positively correlated to the feedstock particle size, where x_2 for the largest particle sizes, 2-2.8 mm, is approximately double the value of the smallest particles, 0.25-0.5 mm. The coefficients of x_2 decreases when the compression speed is increased.

Dashpot

Figure 3.10 shows that the dashpot μ is positively correlated with the particle size, which is similar to the trend for x_2. Considerable differences of the viscosity are observed between the three compression speeds, where the 5 and 10 mm/min coefficients range between 1-4$\cdot 10^9$ Pa·s, while the 1 mm/min

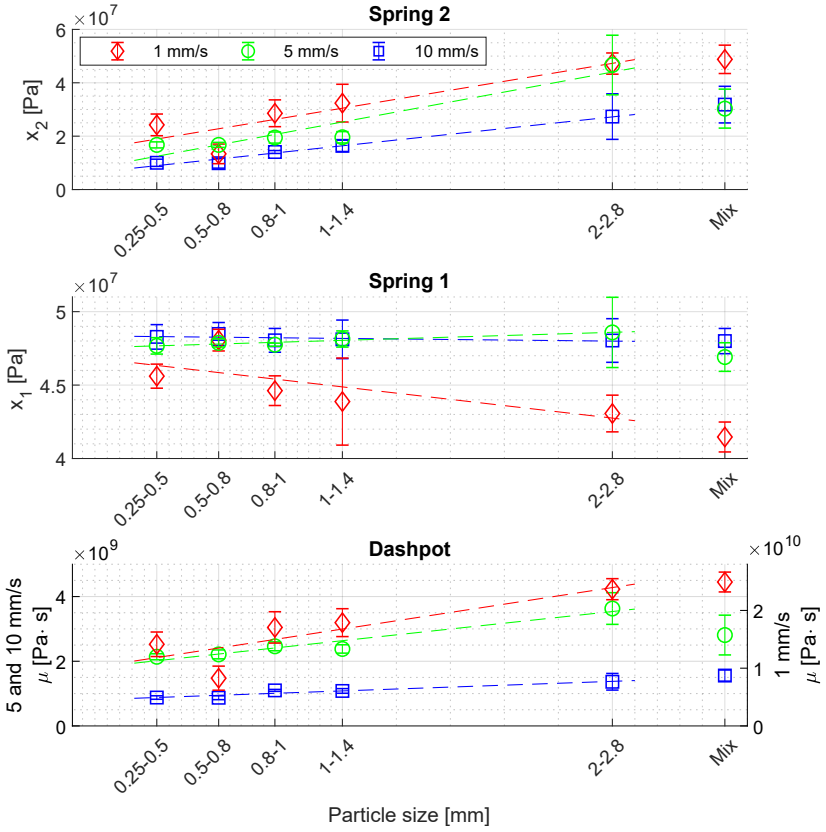

Figure 3.10: Fitted coefficients of x_1, x_2, and μ for particle sizes and compression speeds (figure from paper C [61]).

coefficients are in the range of 1-2.5·10^{10} Pa·s.

Correlation Between Model Elements and Pelleting Properties

The energy and durability data from the single pelleting tests were correlated to the mechanical properties of the model elements. In figure 3.11, a plot of the compression energy and x_2 of the 72 pellets are shown. The linear plots in the figure are fitted to the data for each compression speed.

The plot in figure 3.11 shows a positive linear correlation between the spring coefficient, x_2, and the energy consumed for compressing the energy. It seems valid that x_2 is the parameter that affects the difference in compression energy of the SLS Maxwell model, since the x_1 coefficient, or asymptotic stress of the pellets, is more or less independent of particle size.

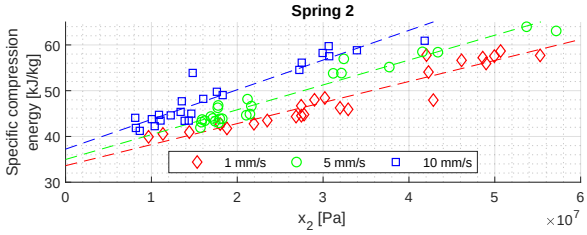

Figure 3.11: Plot of the experimental compression energy and spring coefficient, x_2, for the 72 pellets, and linear plots fitted to the data for each compression speed (figure from paper C [61]).

In figure 3.12, the measured pellet durability and mass-specific work of the dashpot in the SLS Maxwell are plotted.

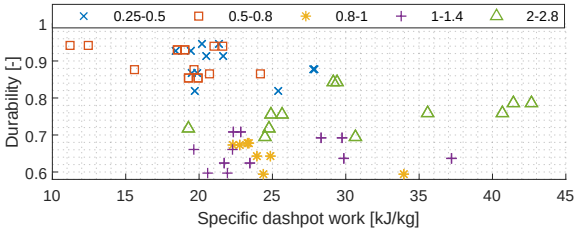

Figure 3.12: Pellet durability vs. mass-specific dashpot work in the SLS Maxwell model for the sieved particle sizes (figure from paper C [61]).

The plot in figure 3.12, shows that the specific dashpot work is lowest for the small particles, while more damping energy is dissipated for the larger particles. Also, the pellets produced with a low specific dashpot work, have the highest durability. The higher specific dashpot work that is exerted when compressing the large particle sizes can be caused by the larger particles storing more elastic energy, which is released as mechanical interlocking and plastic deformations of the particles.

Contribution

The constitutive SLS Maxwell model, presented in paper C, is capable of simulating both the compression and stress relaxation of the spruce particles. The primary contributions of the study are as follows:

- Presentation of an SLS Maxwell model for simulating both the compression and stress relaxation in biomass.
- A pseudo spring porosity is presented for modeling the nonlinearity of the feedstock properties during compression.
- Rheological parameters are derived for different particle sizes of spruce.
- Spring coefficient 1 of the model, composing the asymptotic level of the residual stress, is independent of the feedstock particle size.
- Spring coefficient 2 of the model is positively correlated to the compression energy.
- The mass-specific dashpot work exerted during the compression and stress relaxation is lowest for the small particles, which also produced the pellets with the highest mechanical durability.

The capability of the model to simulate the time-dependent stress relaxation of the compressed feedstock may be utilized in future studies for creating more detailed simulations of the pressure in the press channel of the die, such as the 1D model presented in chapter 2 of this thesis. Furthermore, such simulations may be used for estimating the residual stresses of the pellets when exiting the die, which has been shown to correlate negatively with the pellet durability.

Chapter 4

Effect of the Press Channel Inlet and the Feedstock Layer Shapes in Pellets

In this chapter, the effect of the inlet design of the press channel is investigated. A Computational Fluid Dynamic (CFD) model is set up to simulate the flow, or deformation, of compressed feedstock layers in press channel inlet. Results from experimental single pelleting tests using different combinations of the die inlet angle, β, and depth, h, are presented, together with a novel method to measure the layer shapes in pellets.

4.1 Press Channel Inlet and Feedstock Layer Deformation

The few studies focusing on the press channel inlet have shown, that the inlet affects the energy consumption and pellet durability. The effect on energy consumption was shown via experimental single pelleting tests by Nielsen et al. [25], but also the experimental results for the 1D model, included in this thesis and paper A, showed that the energy consumption varied from 37 to 48 kWh/ton for four different inlet designs.

Other studies have presented results of the inlet's effect on pellet durability. Winter [31] found via single pelleting tests, that an inlet with $\beta = 28^\circ$ produced pellets with higher durability than pellets produced in dies with lower values of β. Winter [31] argued the feedstock in the pellets produced from the $\beta = 28^\circ$ die was more interwoven than the pellets produced in the other dies. Mišljenović et al. [66] observed differences in the breaking

behavior of pellets produced in a $\beta = 37.6^\circ$ die and a pellet produced via compression in a pure cylindrical channel. The ends of the pellets produced in the $\beta = 37.6^\circ$ die had a parabolic shape, while the pellets produced in the cylindrical channel had flat ends. Via three-point bending tests [67], Mišljenović et al. [66] found the pellets from the $\beta = 37.6^\circ$ die, being more durable and better bonded than the pellets from the cylindrical channel.

Generally, all the results from existing studies of the press channel inlet, are based on quantitative analyzes of experimental tests, while no qualitative analyzes of the press channel inlet have been presented. The lack of qualitative analyzes is probably caused by the difficulty of visualizing the process in the press channel, especially in pellet presses, but also in single pelleting tests. Other similar industries as tablet production [68] and metal extrusion [69] have used Computational Fluid Dynamics (CFD) for simulations of flow fields, to understand and optimize their processes. However, to the knowledge of the authors, the CFD technique or other Computer-Aided Engineering tools have not been used for simulation of the pelleting process.

Die Surface

The design parameters of the press channel inlet also affect the design of the die surface. The die surface can be split into three types of area, as described in paper B; active area, transition area, and inactive area, which are shown in figure 4.1.

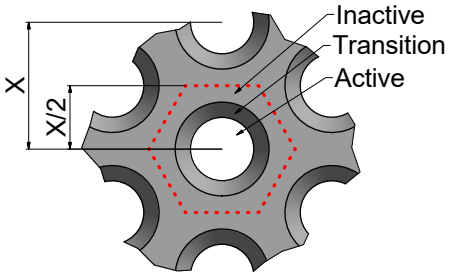

Figure 4.1: Figure from paper D. Sectional view of a die surface with a hexagonal distribution of press channels. The designated press area for a single channel is marked by the red dotted line, where X is the distance between centers of the press channels (figure from paper D [70]).

In figure 4.1, a sectional view of a pellet press die is illustrated, where the active area, or opening area, is the total area composed by the press channels, defined as the product of the cross-sectional press channel area and the number of press channels. The transition area is the projected area of the countersink, and the inactive area is the remaining area between the press channel inlets. As described in section 1.3, the active area usually composes 30-40% of the die area, but to the knowledge of the authors, no numbers are

available for the transition and inactive area. The inlet design affects the ratio of inactive and transition area on the die surface since the transient area is directly correlated to inlet dimensions, β, and h.

4.2 CFD Model

In paper D, CFD simulations of the feedstock motion on the die surface and in the press channel inlet are presented.

The assumptions for the model are as follows:

- Steady-state model, and thereby neglecting the start-stop motion of feedstock in the press channel.
- The feedstock is modeled as an isotropic continuum, and thereby neglecting the effects of fiber orientation [28] or varying particle sizes.
- Isothermal conditions, and thereby neglecting frictional heating from the die walls.

The model is based on a 2D-axis symmetric representation of a press channel, where the axis in the center of the press channel. The model geometry and the applied boundary conditions are shown in figure 4.2.

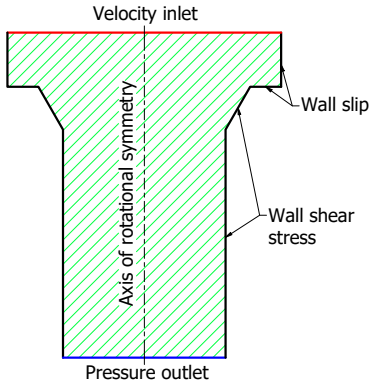

Figure 4.2: 2D axis-symmetric geometry of a die with the applied boundary conditions, where the wall slip is $\tau_w = 0$ Pa, and the wall shear stress is $\tau_w = 10^7$ Pa (figure from paper D [70]).

The CFD model is based on the continuity equation in equation 4.1 and the momentum equations in equation 4.2.

$$\frac{1}{r}\frac{\delta(rv_r)}{\delta r} + \frac{\delta v_z}{\delta z} = 0 \tag{4.1}$$

$$\rho\left(v_r\frac{\delta v_r}{\delta r}+v_z\frac{\delta v_r}{\delta z}\right)=-\frac{\delta p}{\delta r}+\eta\left[\frac{1}{r}\frac{\delta}{\delta r}\left(r\frac{\delta v_r}{\delta r}\right)-\frac{v_r}{r^2}+\frac{\delta^2 v_r}{\delta z^2}\right] \tag{4.2a}$$

$$\rho\left(v_r\frac{\delta v_z}{\delta r}+v_z\frac{\delta v_z}{\delta z}\right)=-\frac{\delta p}{\delta z}+\eta\left[\frac{1}{r}\frac{\delta}{\delta r}\left(r\frac{\delta v_z}{\delta r}\right)+\frac{\delta^2 v_z}{\delta z^2}\right] \tag{4.2b}$$

In equation 4.1 and 4.2, ρ is the density, r and z are the radial and axial orientation of the press channel, v_r and v_z are the radial and axial velocity, p is the pressure, and η is the non-Newtonian viscosity.

The feedstock viscosity is modeled as a simplified Bingham plastic, which is a commonly used idealization of viscoplastic fluids [71]. The Bingham model utilizes a yield stress criterion, τ_0, where the fluid behaves as a rigid solid when the shear stress is below τ_0, and assumes fluid behavior when the shear stress exceeds τ_0 [72].

The Bingham model is reduced by setting the viscosity to zero in the applied Bingham model, causing the viscosity model to depend on τ_0. The viscosity model is defined in equation 4.3.

$$\eta=\begin{cases}\frac{\tau_0}{\dot{\gamma}} & \text{for } \dot{\gamma}\geq\dot{\gamma}_c\\ \tau_0\frac{(2-\dot{\gamma}/\dot{\gamma}_c)}{\dot{\gamma}_c} & \text{for } \dot{\gamma}<\dot{\gamma}_c\end{cases} \tag{4.3}$$

In equation 4.3, $\dot{\gamma}$ is the shear rate, and $\dot{\gamma}_c$ is the critical shear rate [73].

Model Settings

The model parameters are listed in table 4.1. A wall slip condition with constant shear stress, τ_w, is applied to the wall of the press channel. The slip condition is commonly used for simulations of viscoplastic fluids [74,75]. The feedstock is assumed to move as a plug in the press channel, causing τ_w is set lower than τ_0 of the feedstock. Further information about the CFD model setup can be found in paper D.

Table 4.1: Settings used in the CFD simulations.

Model settings	
Yield stress, τ_0	$1.1\cdot10^7$ Pa
Critical shear rate, $\dot{\gamma}_c$	10^{-2} s^{-1}
Density	1100 kg·m^{-3}
Wall shear stress, τ_w	10^7 Pa
Velocity inlet	1.25 mm· s^{-1}
Pressure outlet	0 Pa

4.3 Layer Profile Analysis

Experimental Pelleting Test and Layer Profile Analysis

Single pelleting tests with spruce *(Picea abies)* was performed, where seven different inlet designs were tested. Information about the properties of the spruce is found in paper D. The purpose of the tests was twofold:

1. Measure the energy consumption for continuous pelleting in the dies, and measure the durability of the produced pellets.
2. Analyze the shapes of the feedstock layers in the produced pellets, which are used as validation of the CFD model.

In figure 4.3, drawings of the single pelleting equipment are shown.

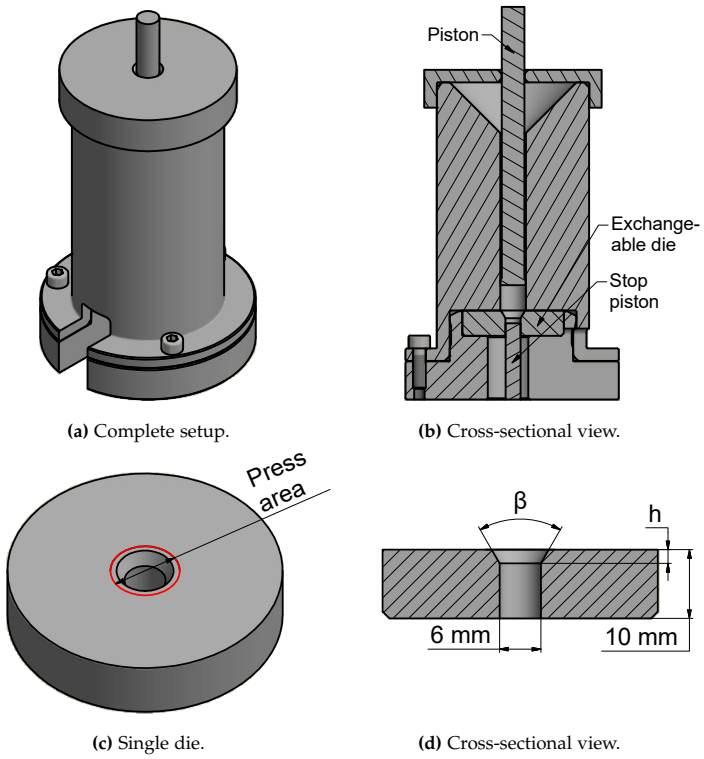

(a) Complete setup.

(b) Cross-sectional view.

(c) Single die.

(d) Cross-sectional view.

Figure 4.3: Illustration of the single pelleting unit and single dies (figure from paper D [70]).

The single pelleting setup in figure 4.3 was designed and produced for this test. The dies were selected to represent different values of β and h. A design parameter, AR, representing the ratio of inlet and transition area

to the total area of the die surface, was set up for comparison of the dies. Calculation of AR is shown in equation 4.4

$$AR = \frac{active\ \ area + transition\ \ area}{total\ \ area} \tag{4.4}$$

The design parameters of the tested dies are listed in table 4.2.

Table 4.2: Table from paper D. Dimensions of exchangeable die units. The length of the dies is 10 mm and the diameters is 6 mm.

Die	β [°]	h [mm]	AR [−]
1	-	0	0.35
2	60	1.58	0.60
3	60	2.63	0.80
4	60	3.55	1.00
5	100	0.77	0.60
6	100	1.27	0.80
7	100	1.72	1.00

A detailed description of the test procedure for the continuous pelleting test is found in paper D, where:

- The energy consumption of the continuous pelleting test was calculated from the force vs. displacement of the pressing piston when pressing feedstock layers into the die.
- The mechanical durability was measured via tumbling of single pellets [76], where three pellets were produced from each die.
- The shape of the layer profiles was evaluated by pressing five layers of alternately blue and red colored spruce into the die. After that, the cast of colored feedstock layers sitting in the die was ejected and embedded in epoxy. After hardening, the embedded pellets were sanded, such that a cross-sectional view of the die-cast was visible, as shown in figure 4.4a.

By using image processing, the profiles between the colored feedstock layers were evaluated from photos of the sanded die casts. Figure 4.4 shows the steps of the image processing.

In figure 4.4, the first processing step is cropping the blue/green colored layers of the pellet, as shown in figure 4.4b. Next, a binary image is generated in figure 4.4c, and finally, all small regions are filtered out in figure 4.4d. The layer profiles of the pellets are then evaluated from the edge between the bottom blue and red layer.

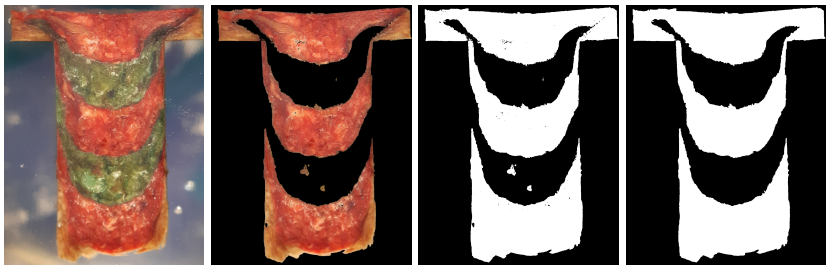

(a) Raw photo. **(b)** Cropped. **(c)** Binary. **(d)** Filtered binary.

Figure 4.4: Image processing of the cast part from die 1 (figure from paper D [70]).

Experimental Results

Energy Consumption and Pellet Durability

The energy consumptions from the single pelleting tests and the measured pellet durabilities are shown in figure 4.5, where the error bars in figure 4.5a represent the standard deviations of the measurements.

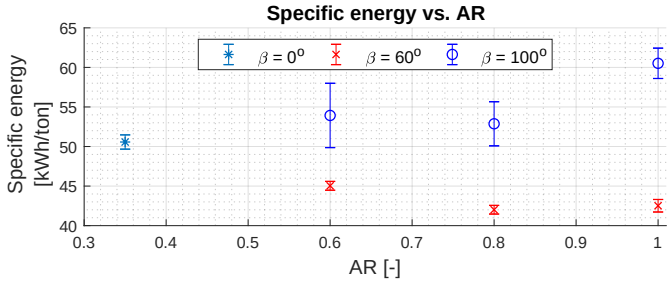

(a) Specific energy consumption for the tested dies.

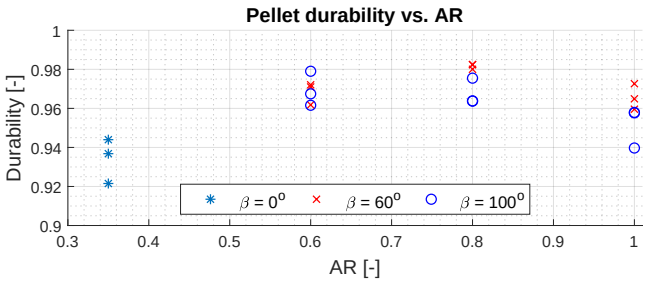

(b) Durability of pellets produced in the tested dies.

Figure 4.5: Experimental results of energy and durability (figure from paper D [70]).

The mass-specific energy consumptions from the single pelleting tests are represented in the unit of kWh/ton, which is often used by the industry. The

energy consumptions in figure 4.5a show that the $\beta = 100^\circ$ die consumes more energy compared to the $\beta = 60^\circ$ dies, while the consumption of the blank die with $\beta = 0^\circ$, is between the $\beta = 60^\circ$ and $\beta = 100^\circ$ dies. Figure 4.5a also shows that the energy consumption for the $\beta = 60^\circ$ decreases when AR increases from 0.60 to 0.80, and the die with $AR = 1.00$ consumes similar to the 0.80 die. An opposite effect of the AR is observed for the $\beta = 100^o$ dies, where the highest energy consumption is observed for the die with an AR of 1.00.

The measured pellet durabilities in figure 4.5b, shows that the durability is highest for the pellets produced in the dies with an AR of 0.60 and 0.80, and the durability is more or less independent of the tested values of β. The lowest durability was measured for the pellets that were produced in the $\beta = 0^\circ$ die. It was observed, that the pellets produced in the $\beta = 0^\circ$ die broke into two smaller pellets during the pellet tumbling, while all other pellets remained in one pellet. The broken pellets might be a reason for the lower durability values of the $\beta = 0^\circ$ pellets.

Layer Profiles

The photos of the embedded and sanded pellets are shown in figure 4.6.

The layer profiles from the pellets in figure 4.6 are plotted in figure 4.7. The general observations from figure 4.7 are that by increasing the AR of the dies, the layer profiles become steeper from the perimeter of the pellet towards the pellet center, and the $\beta = 0^\circ$ die produces a layer profile that is relatively flat in the center and steep near the perimeter. An interesting observation from the photos in figure 4.6, is the stagnant regions of the pellets, that are observed by the uncolored spruce in the inlets of the dies. Stagnant regions are observed in the inactive area for die 1, 2, and 4, which are the dies with the lowest AR. Also, in the inlet of die 6 and 7, with $\beta = 100^\circ$, the stagnant feedstock is observed, which creates a new secondary inlet angle defined by the interface between moving and stagnant feedstock.

(a) Die 1.

(b) Die 2.

(c) Die 3.

(d) Die 4.

(e) Die 5.

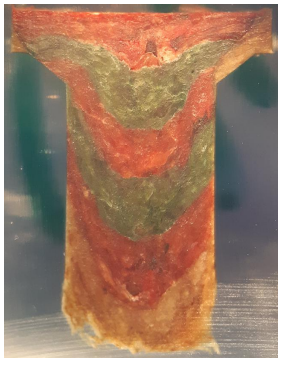

(f) Die 6.

(g) Die 7.

Figure 4.6: Photos of the casts from the dies (figure from paper D [70]).

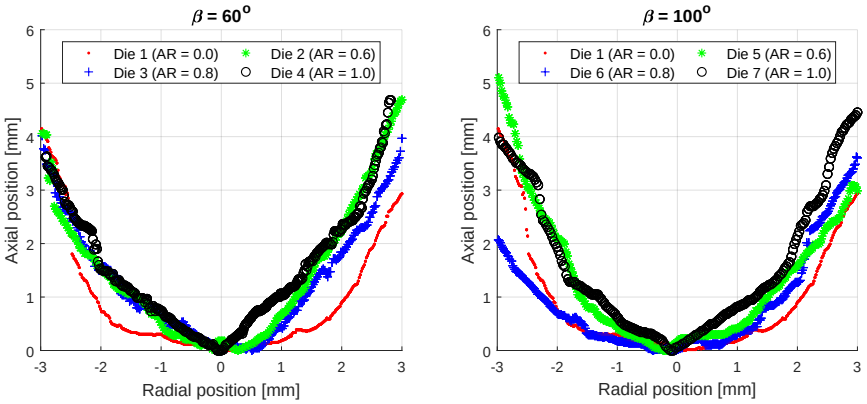

(a) Layer profiles from dies with $\beta = 60°$.

(b) Layer profiles from dies with $\beta = 100°$.

Figure 4.7: Layer profiles found via image processing of the pellets produced in the tested dies (figure from paper D [70]).

In figure 4.8, a photo before and after tumbling of pellets from the blank die and die no. 4 ($\beta = 60°$ and $AR = 1.00$) are shown. The end shapes before and after the tumbling of the two pellets show that the pellet produced in the blank die has lost a significant amount of feedstock during tumbling, compared to the pellet produced in die no. 4. The end shapes of the tumbled pellets in figure 4.8 from the two dies, are similar to the layer profiles in figure 4.7. The similarity could indicate that the intersection between two feedstock layers is where the pellet breaks. However, the pellet from the blank die, which has a layer profile with a relatively flat center and steep edges, appear to break along the flat center but creates a secondary break profile at the edge of the pellet. During tumbling of the pellets produced in the blank die, the feedstock that is located between the breaking profile and layer profile is released from the pellet, which causes lower durability, as seen in figure 4.5b.

The breaking profile and layer profile of the pellet produced in die no. 4 are very similar before and after tumbling, resulting in better durability.

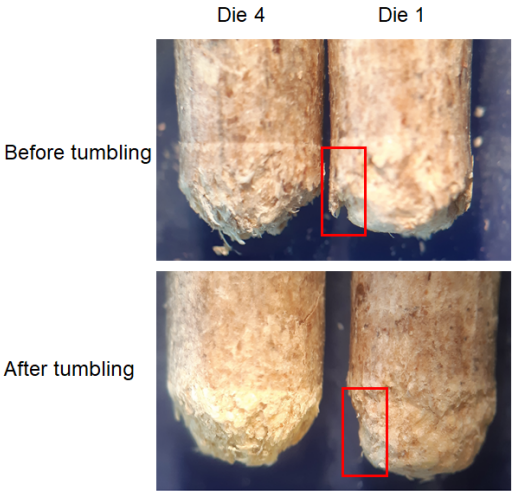

Figure 4.8: Comparison of a pellet from the blank die and die no. 4, before and after tumbling. The red marker shows the region with a significant difference in pellet shape before and after tumbling (figure from paper D [70]).

Simulation Results

In figure 4.9, three contour plots from the CFD simulation of die no. 2 are shown. Figure 4.9a shows the simulated feedstock velocity, where it is seen that the feedstock moves as a plug in the press channel. Also, the stagnant region on the die's inactive area is observed, which is similar to the photo in figure 4.6b. The edge of the inactive area is also seen by the simulated shear rate in figure 4.9c, where a high shear rate is observed at the interface between the stagnant and moving feedstock. The dark blue areas in figure 4.9c indicate that the feedstock moves as a solid, and thereby obey $\dot{\gamma} < \dot{\gamma}_c$.

The simulated retention time is shown by colored streamlines in figure 4.9b. The simulated feedstock layer profiles are derived as the feedstock position at the retention time before the feedstock exits the model domain.

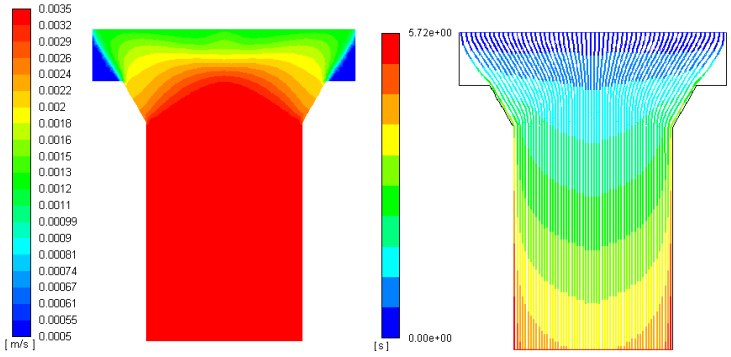

(a) Velocity.

(b) Streamlines with colors representing the feedstock retention time.

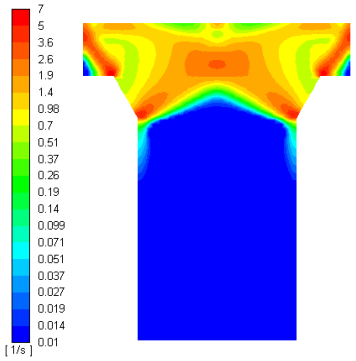

(c) Shear rate.

Figure 4.9: CFD simulation results of die no. 2, $\beta = 60°$ and $AR = 0.60$ (figure from paper D [70]).

The experimental and simulated layer profiles are plotted in figure 4.10,

showing that the CFD models are capable of qualitatively reproducing the experimental layer profiles. However, the asymmetry of the experimental layer profiles is not captured by the model, which is likely caused by the feedstock not behaving as a continuum, as assumed in the CFD model.

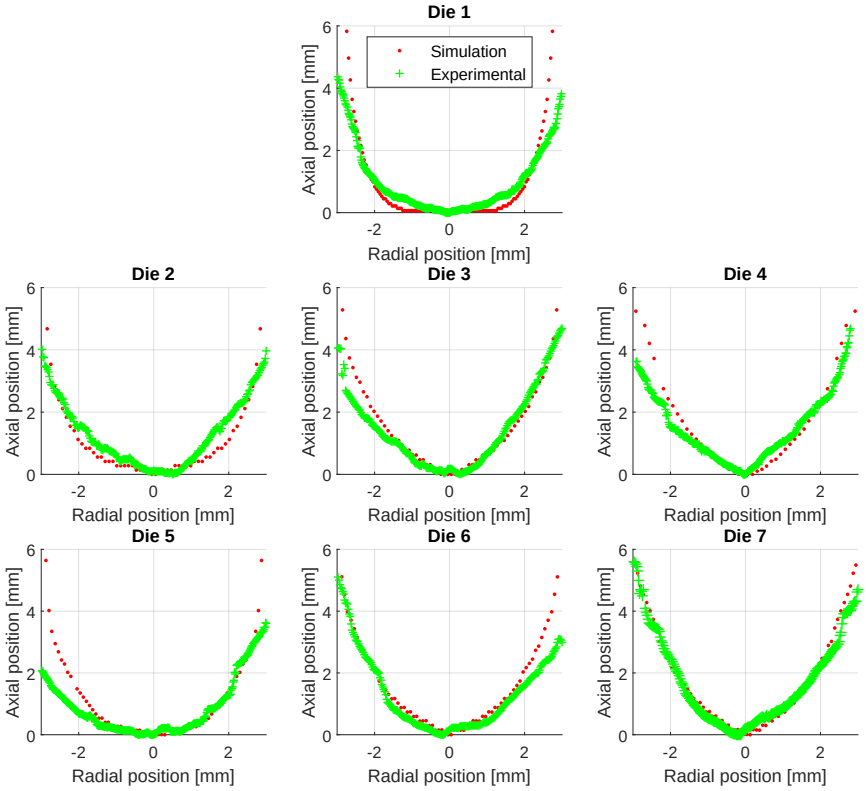

Figure 4.10: Comparison of experimental and simulated layer profiles in the pellets (figure from paper D [70]).

Effect of Layer Profile

To quantify the differences in layer profiles produced from the seven dies, the kurtosis [77] of the layer profiles is calculated, by assuming the layer profiles as an upward-facing distribution. A description of the kurtosis calculation is found in paper D.

Figure 4.11 shows two plots with the kurtosis, the pellet durability, and AR of the dies.

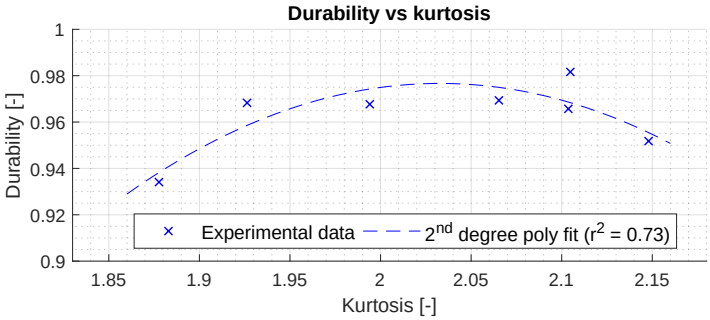

(a) Plot of kurtosis and pellet durability.

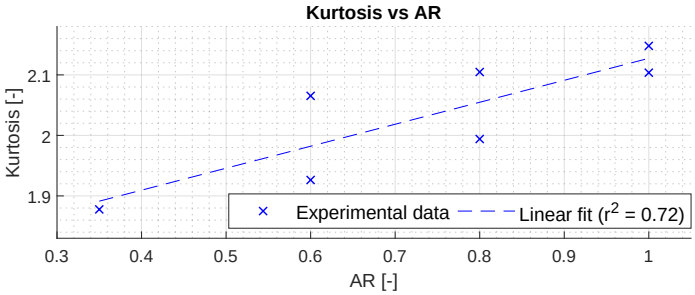

(b) Plot of layer profile kurtosis and AR.

Figure 4.11: Plots of the profile layer kurtosis (figure from paper D [70]).

In figure 4.11a, a 2nd degree polynomial function is fitted to the kurtosis and the pellet durability data. The fitted function has a $r^2 = 0.73$. Figure 4.11a shows that the pellets with a layer profile kurtosis of 2.00-2.05 have the highest durability.

Figure 4.11b shows a linear correlation between AR and the kurtosis. The fitted linear function with $r^2 = 0.72$ and a p-value = 0.016, meaning that there is a significant correlation between AR of the die design and the layer profile kurtosis.

Contribution

The CFD model presented in paper D is capable of simulating the feedstock motion in press channel, which has been validated from experimental observations of the layer shapes in pellets. The primary contributions of the study are as follows:

- The feedstock motion in press channels can be simulated with a CFD model using a simplified Bingham viscosity model, which can simulate where the feedstock behaves as a solid or as fluid in the press channel.
- The design parameter AR, which specifies the ratio of active and transition area on the die, correlates linearly with the kurtosis of the layer profiles in the pellets. The kurtosis correlates to the durability of the pellets, where the highest durability was produced with a kurtosis of 2.00-2.05.
- Regions with stagnant feedstock was observed on the inactive area of the tested dies, and in the inlet part of two dies with $\beta = 100^\circ$ and AR of 0.80 and 1.00.
- From continuous single pelleting tests with seven different dies, it was found that the dies with $\beta = 60^\circ$ consume less energy compared to the $\beta = 100^\circ$ dies and that the $\beta = 60^\circ$ dies with an AR of 0.80 and 1.00 had the lowest energy consumption.
- The highest pellet durability was produced with the dies having an AR of 0.60 and 0.80, while no considerable difference in pellet durability was found between the $\beta = 60^\circ$ and $\beta = 100^\circ$ dies.

The CFD model in paper D provides a basis for future simulations, which can be extended to simulate patterns of press channels in the die, and thereby investigate the motion of the feedstock between the press channels, which have not been done before. Also, a method should be developed for measuring the yield stress, τ_0, for simulating different feedstock species.

Chapter 4. Effect of the Press Channel Inlet and the Feedstock Layer Shapes in Pellets

Chapter 5

Process Parameters of the Pellet Press

In this chapter, the effects of the thickness of the feedstock layer on the die and the influence of the gap size between die and roller are analyzed, where a pilot-scale ring die pellet press was set up for experimental testing.

5.1 Feedstock Motion in the Press Channel

The results of the 1D model in chapter 2, showed that the simulated energy consumption were 2.2-2.5 times higher than the energy consumption found from the experimental single pelleting tests. The overestimation of the energy consumption might be caused by the assumption of a steady-state process, where the pelleting force is constant. However, from single pelleting tests, the applied force for pressing a feedstock layer into the press channel was found to vary. Figure 5.1 shows the applied force that has been recorded while pressing one layer of feedstock into a single press channel.

The force recording in figure 5.1 is split into three phases:

1. Feedstock is being compressed and is not being conveyed in the channel. In this phase there is a static friction between the channel wall and the forming pellet.

2. When reaching a peak in applied force, the wall friction shifts to a transition phase, which initiates the motion of feedstock in the press channel. During the transition phase, the force decreases. The transition phase is a complex interaction of multiple mechanisms, such as the stick-slip phenomenon, which is an effect of alternating sticking and

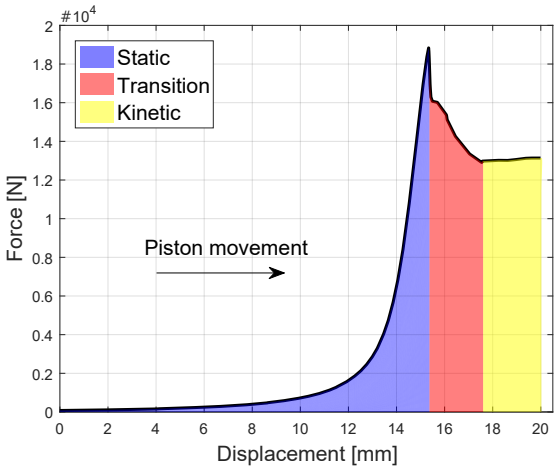

Figure 5.1: Force recordings from pelleting of spruce in a single pellet press (figure from paper B [15]).

slipping of the feedstock, caused by the system properties of elasticity, damping, and inertia [78].

3. In the final phase, the force reaches a steady level with kinetic friction, where feedstock is pressed through the press channel.

In figure 5.1, the frictional work in the press channel is represented by the colored areas in the transition and kinetic phases, while the marked area in the static region can be interpreted as the compressional work.

The 1D model calculates the pelleting force as the peak force, measured at the transition between the static and transition phase in figure 5.1, but it does not account for the effects of the lower friction in the kinetic phase.

Pellet Press Layer Thickness and Roller Gap

In figure 5.2a, the ring die and the two rollers of the pellet press that is used for the pelleting tests in paper E are illustrated. Figure 5.2b illustrates the feedstock layer in front of the roller and the roller gap between die and roller. The mass of feedstock being pressed into the press channels per roller passing is directly correlated to the thickness of the feedstock layer.

By increasing the thickness of the feedstock layer, the duration of the transition and kinetic friction phase is extended, and the number of start-stops in the press channel is reduced pr. unit mass of pelleted feedstock. Reducing the number of start-stops could decrease the mass-specific energy consumption, which also was commented in a study by Winter [31]. However, minimal research on the effect of the feedstock layer has been performed. Wu et al. [80]

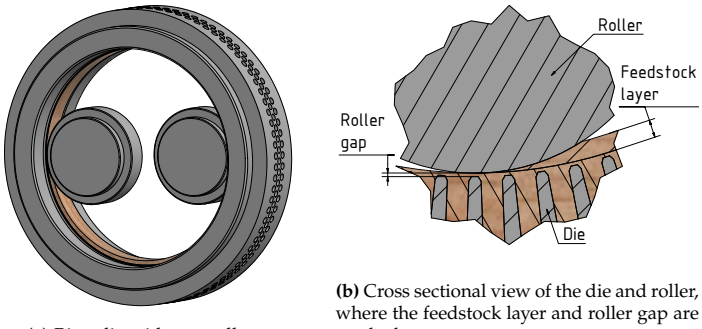

(a) Ring die with two rollers.

(b) Cross sectional view of the die and roller, where the feedstock layer and roller gap are marked.

Figure 5.2: Illustration of die and rollers, and the two operational parameters, feedstock layer, and roller gap (figure from paper E [79]).

studied the effect of rotational die speed with a constant feedstock mass flow rate. They found the energy consumption of the pellet press to increase with the die speed, which is correlated with the thickness of feedstock layer.

The feedstock layer is quantified as the mass of feedstock, m_f, that is pressed into one press channel at each roller pass, and the corresponding thickness of the feedstock layer, h_f.

The mass of the feedstock layer is calculated via equation 5.1. In the calculation of m_f, it is assumed that the feedstock is distributed evenly on the die surface.

$$m_f = \frac{\dot{m}}{N_r \cdot \omega_d \cdot N_{ch}} \tag{5.1}$$

In equation 5.1, N_r is the number of rollers in the pellet press, ω_d is the rotational frequency of the die, $\dot{m}$ is the feedstock mass flow, and N_{ch} is the number of press channels in the die.

The thickness of the feedstock layer, h_f, is calculated via equation 5.2.

$$h_f = \frac{\dot{m}}{N_r \cdot \omega_d \cdot \rho_b \cdot A_d} \tag{5.2}$$

In equation 5.2, A_d is the area of the die's inner surface, and ρ_b is the bulk density of the feedstock.

Pelleting Energy Calculation

Based on the static and kinetic friction phases in figure 5.1, a simple expression for calculating the energy consumption is proposed, which is derived from the simplified friction plot in figure 5.3.

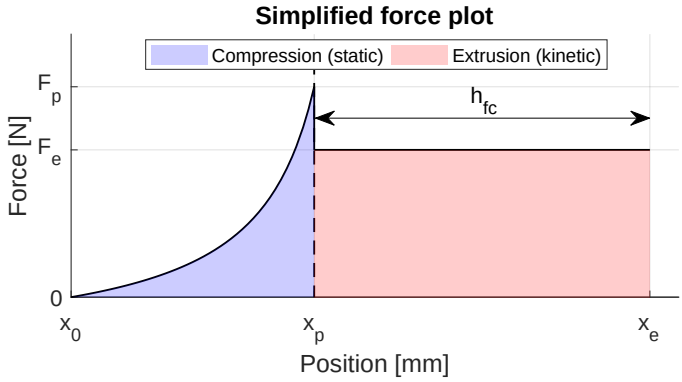

Figure 5.3: Illustration of the pelleting force with a simplified transition between the static (compression) and kinetic (extrusion) phase (figure from paper E [79]).

In figure 5.3, F_p is the static pelleting force and x_p is its corresponding position, F_e is the kinetic pelleting force and x_e is the position where the press stops. The difference between x_p and x_e can be interpreted as the thickness of the compressed feedstock layer, h_{fc}.

From the simplified friction plot in figure 5.3, the mass-specific energy consumption, w, is calculated using equation 5.3.

$$w = \frac{E_c + F_e \cdot h_{fc}}{m_f} \tag{5.3}$$

In equation 5.3, E_c is the energy required to compress the feedstock. In figure 5.3, E_c is equal to the blue-colored area in the compression phase, and the product of F_e and h_{fc} is the red-colored area, which is the friction work. In this study, the values for h_f are used instead of h_{fc}, since the compressed heights of the feedstock layers are unknown.

The expression of h_f is directly correlated to m_f, causing that the mass-specific friction work in equation 5.3 is constant, if assuming F_e to be independent of m_f. Hence, it is only the compression energy that depends on m_f, as shown in equation 5.4.

$$w = \frac{E_c}{m_f} + F_e \cdot \frac{N_{ch}}{A_d \cdot \rho_b} \tag{5.4}$$

Pellet Durability Calculation

Handling and transportation of pellets include impacts and wear of the pellets, which may release particles from the pellets ends, reducing the durability of the pellets. Observations from the analysis of feedstock layer profiles, described in section 4.3, showed that the shapes of the pellet ends were

similar to the layer profiles and that the pellets tend to break between the feedstock layers. Based on this observation, the number of compressed feedstock layers in a pellet is thought to affect the pellet durability, since more layers could cause more pellet breaks. To test this hypothesis, a simple empirical expression of the pellet durability is set up in equation 5.5, where m_f is inversely proportional to a fitting parameter, a.

$$\text{Durability} = 100 - \frac{a}{m_f} \tag{5.5}$$

The expressions set up in equation 5.3 and 5.5, are fitted to experimental data from pelleting tests, to investigate if the proposed equations can be validated and if the effects of the feedstock layer are as assumed.

5.2 Pellet Press Set Up and Tests

An experimental setup with a 15 kW ring die pellet press was build as a part of the work in this Ph.D. project. The pellet press is equipped with frequency drives on the main motor and feed-screw motor, to allow a controlled variation of the rotational die speed and mass flow rate of the feedstock. Figure 5.4a shows a photo of the setup, where the feedstock is conveyed from the hopper to the pellet press. On top of the pellet press, the feedstock is fed into a conditioner, where steam can be added to the feedstock, which is supplied from a 15 kW electrical steam boiler. After the conditioner, the feedstock is feed into the press chamber of the die, which is shown in figure 5.4b. In the press chamber, the scrapers' positions are adjusted to distribute the feedstock evenly in front of the rollers. The gap between die and roller is adjusted by the angular position of the latch on each roller.

After the pellet press, the pellets are conveyed to a pellet cooler, where a suction hose generates an airflow through the pellet bed and cools the pellets.

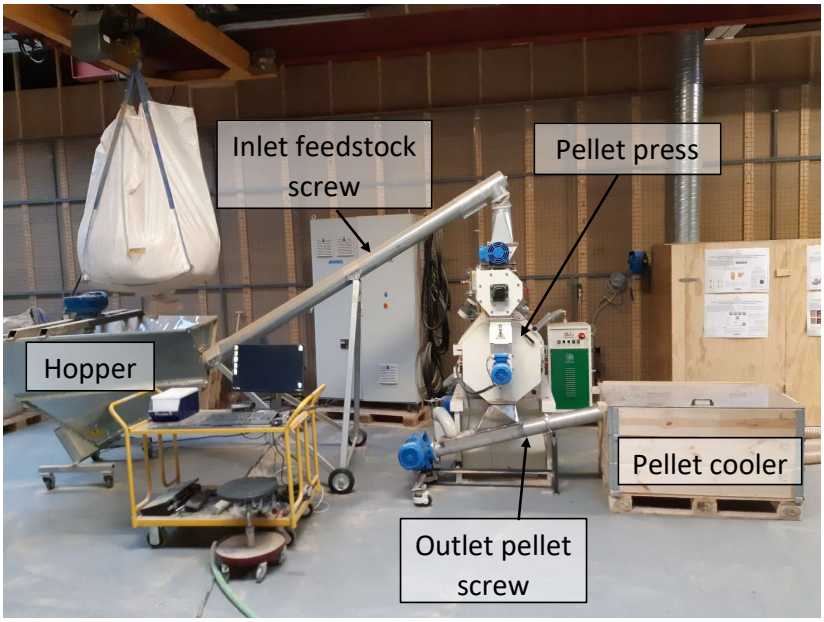

(a) Pellet press test setup (figure from paper E [79]).

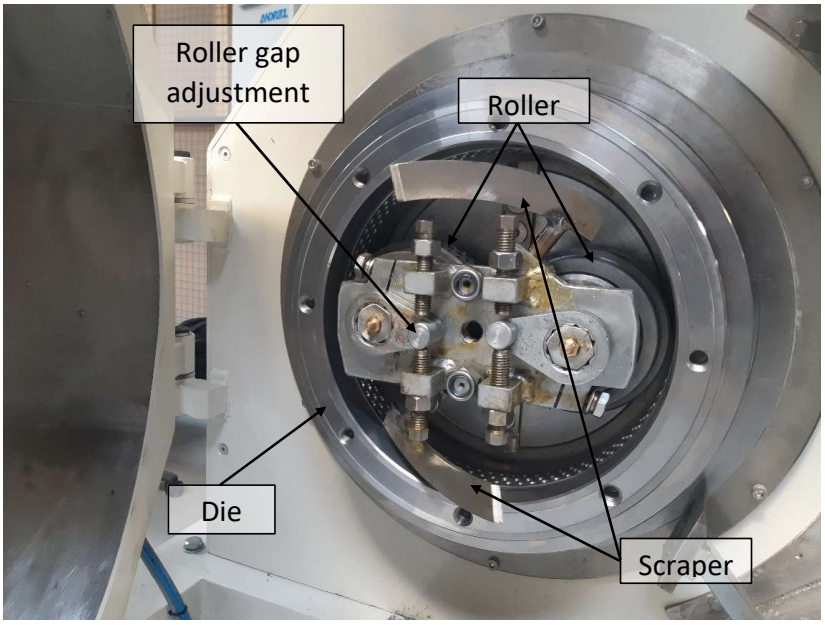

(b) Press chamber of the pellet press.

Figure 5.4: Photos of the pellet press setup and the press chamber.

Pelleting Tests

Pelleting test was performed with spruce, with a moisture content of approximately 9.9% on wet basis (w.b), and no steam conditioning.

The specifications and applied settings of the pellet press and die for the pelleting tests are listed in table 5.1. A full-factorial test of rotational die speed, feedstock mass flow rate, and roller gap was performed, where each factor was tested at three levels:

- Rotational die speed: 60 Hz, 48 Hz, and 36 Hz, corresponding to 5.10 m/s, 4.08 m/s, and 3.06 m/s. Plus, two tests at 24 Hz (2.04 m/s).
- Feedstock mass flow rate: 90 kg/h, 120 kg/h, and 150 kg/h.
- Roller gap: 0.2 mm, 0.9 mm, and 1.6 mm.

Due to problems with the frequency converter, only two tests were performed at a rotational die speed of 24 Hz. A total of 29 pelleting tests were performed, and approximately 1.5 tons of pellets were produced.

Table 5.1: Pellet press and die configurations (table from paper E [79]).

Pellet press	
Feed-screw capacity	150 kg/h
Press motor power	15 kW
No. of rollers	2 pcs.
Roller gap	0.0-1.6 mm
Die speed	3.1-5.1 m/s
Inner die diameter	250 mm
Die width	26 mm
No. of press channels	252 pcs.
Die press channels	
Diameter	6 mm
Length	35 mm
Inlet angle, β	60°
Inlet depth, h	1.6 mm

During the tests, the power consumption of the pellet press main motor was monitored and recorded for five minutes when reaching a steady level for each test. A sample of pellets was collected from each test to measure the bulk density of the pellets according to ISO 17828:2015 [81] and the feedstock mass flow rate. The mechanical durability of the pellets was measured according to ISO 17831-1:2015 [82] and was measured three times for each test sample.

A comparison of pellet length was performed by measuring the average pellet length for each test using image processing. The image processing was performed by spreading a sample of pellets on a white paper with a size of 297x210 mm which was photographed with a resolution of 4608x3456 pixels. The software Matlab was used to process the pellet images. The pellet lengths were calculated by measuring the longitudinal and diametral dimensions of each pellet, and assuming the average diametral dimension of the pellets to be 6 mm. The image processing steps are illustrated in figure 5.5. Figure 5.5a and 5.5b show the raw photo of the pellets and the corresponding binary image. The red dots in figure 5.5b indicates that the distance between two pellets is too small, and thereby are excluded from the analysis. The distribution of the pellet lengths is shown in figure 5.5c.

The image processing method allows many pellets to be analyzed in a short amount of time compared to manual techniques as caliber measurements. The image processing method requires that the pellets are lying on the side. However, tiny pellets may face an end upwards, and therefore will appear to have a length equal to its diameter.

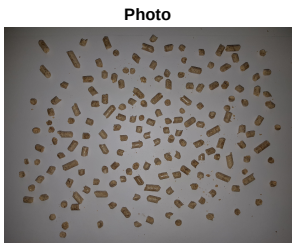

(a) Raw photo of a pellet sample.

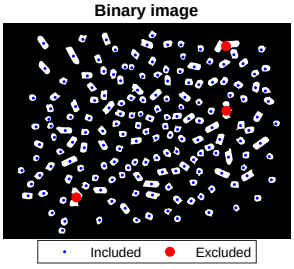

(b) Processed binary image.

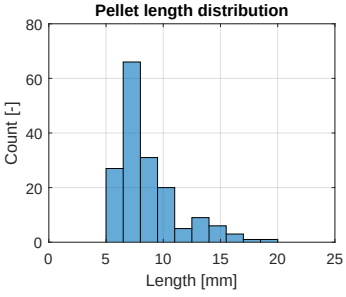

(c) Plot of pellet length distribution.

Figure 5.5: Image analysis of a pellet sample produced with die speed 3.08 m/s, mass flow rate 90 kg/h, and roller gap 0.2 mm (figure from paper E [79]).

Results of Pelleting Tests

The tests with roller gaps of 0.9 mm and 1.6 mm caused vibrations of the pellet press, which increased when the die speed was increased. Hence, the test at 60 Hz with a roller gap of 1.6 mm was suspended, and no pellet durability was measured for this test and the corresponding 48 Hz test. The vibrations might be caused by a roller slip, which appears when the peripheral speed of the roller is lower than the die speed.

Mass-Specific Energy Consumption

The mass-specific energy consumptions from the pelleting tests are plotted in figure 5.6, where equation 5.3 is fitted to the experimental data for each roller gap. The error bars in the figure indicate the standard deviation of the measurements.

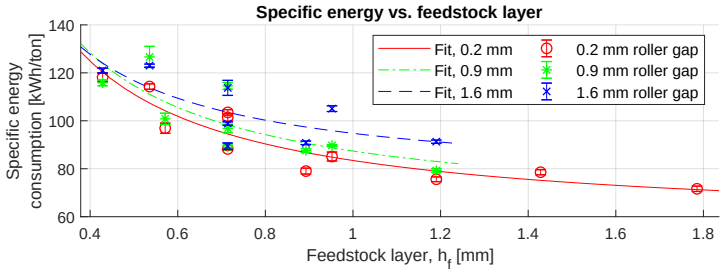

Figure 5.6: Experimental data of the specific energy consumption and plots of equation 5.3 for each roller gap setting (table from paper E [79]).

The plot in figure 5.6 shows that the specific energy consumption of the pellet press decreases when the thickness of the feedstock layer increases. This tendency is observed for all three roller gap settings, where it also is seen that the specific energy consumption increases when the size of the roller gap is increased. The three plots of equation 5.3 in figure 5.6 show the same tendency of energy consumption as the experimental data.

The fitted coefficients of the compression energy, E_c, and the kinetic pelleting force, F_e, in equation 5.3, are listed in table 5.2.

The values of E_c in table 5.2 indicates an increase of compression energy when increasing the roller gap. A thicker layer of the compressed feedstock on the die, when increasing the roller gap, may increase F_p, which increases the compression energy. The fitted values of the kinetic pelleting force, F_e, in table 5.2 is slightly decreasing when the size of the roller gap is increased. This might be caused by differences in the friction force, since the energy consumption increases, and thereby the die temperature is likely to be higher, which may affect the friction. Since the regression of equation 5.3 is based on

Table 5.2: Regression results of equation 5.3 and the experimental data (table from paper E [79]).

Roller gap	Coefficient		r^2	RMSE
	E_c	F_e		
0.2 mm	250.8	0.1241	0.8585	6.2928
0.9 mm	270.0	0.1226	0.6324	10.2289
1.6 mm	327.0	0.0987	0.5842	9.5650

h_f, and not the correct parameter h_{fc}, the coefficients in table 5.2 can only be taken as relative differences when changing the roller gap, and not absolute values. The vibrations that were observed for the 0.9 mm and 1.6 mm roller gap tests might explain the larger error bars for some of the data in figure 5.6, and the lower values of r^2 compared to the roller gap of 0.2 mm in table 5.2.

The general level of the measured specific energy consumptions are higher than the typical 30-60 kWh/ton consumed by industrial pellet presses [21–24], which could be caused by the feedstock not being conditioned before pelleting [20], and differences in the feedstock layer in the pilot-scale pellet press and industrial pellet presses.

Pellet Durability

Figure 5.7 shows a plot of the pellet durabilities and values of m_f, together with three fits of equation 5.5. The error bars represent the standard deviation of the durability measurements.

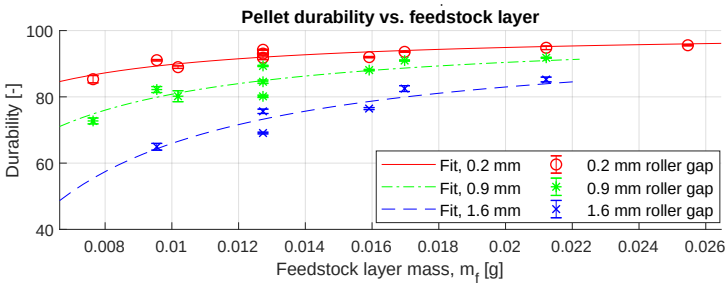

Figure 5.7: Experimental data points of the pellet durability and plots of equation 5.5 for each roller gap setting (table from paper E [79]).

The plot in figure 5.7 shows that the pellet durability increases when the mass of the feedstock layer is increased and that increasing the roller gap decreases the pellet durability. The effect of the roller gap on pellet durability is opposite to what was reported by Kaliyan et al. [18], who stated that the

durability of feed pellets increased when increasing the roller gap up to 2-2.5 mm. The difference might be explained by differences between feed and biomass, where pelleting of feed requires 3-4 times less energy than biomass pelleting [24]. Generally, the durability of the pellets are low compared to the requirements of ISO 17225-2:2014 [10], which is likely caused by the low feedstock moisture content of 9.9% (w.b) [16], and no steam conditioning of the feedstock.

The plots of equation 5.5 in figure 5.7 fits well to the experimental data, suggesting that there is a correlation between the pellet durability and the mass of the feedstock layers in the pellets. The fitted coefficients of a in equation 5.5 are listed in table 5.3.

Table 5.3: Regression results of equation 5.5 and the experimental data (table from paper E [79]).

Roller gap	Coefficient, a	r^2	RMSE
0.2 mm	0.1021	0.8221	1.2867
0.9 mm	0.1921	0.8111	2.7158
1.6 mm	0.3406	0.8784	2.6887

Bulk Density and Pellet Length

Figure 5.8 shows the measured bulk density of the pellet samples. No clear correlation between the bulk density and the feedstock layer was observed. However, the die speed and roller gap showed to affect the bulk density, which is shown by the plot in figure 5.8.

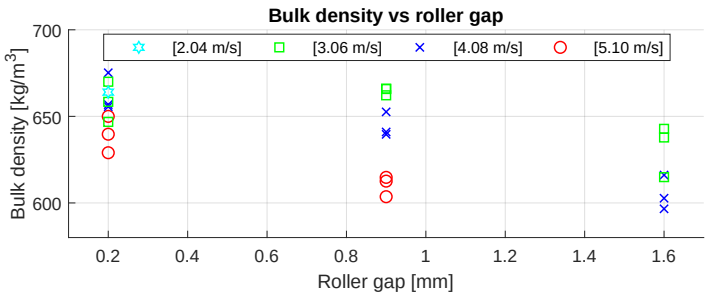

Figure 5.8: Effect of roller gap and die speed on the pellet bulk density (figure from paper E [79]).

Figure 5.8 shows that the bulk density decreases when the die speed and roller gap are increased. Generally, the bulk densities in figure 5.8 fulfill the minimum requirement of 600 kg/m^3 in ISO 17225-2:2014 [10].

The results of the pellet length measurements and corresponding feedstock layers are plotted in figure 5.9.

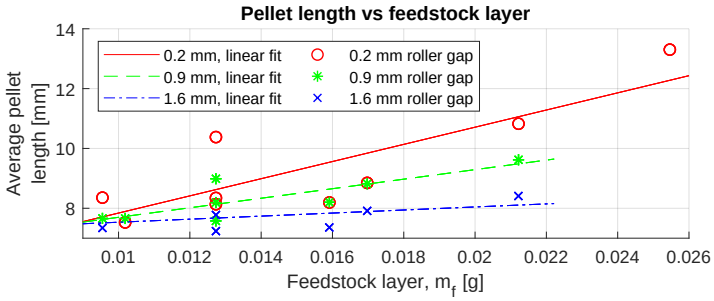

Figure 5.9: Plot of average pellet length and feedstock layer with linear fits for each roller gap size (figure from paper E [79]).

The linear functions in figure 5.9 are fitted to the data for each of the three roller gap sizes. The plot shows that there is a positive correlation between the average pellet length and the feedstock layer, while a negative correlation is observed for the size of the roller gap.

The pellet length is likely correlated to the adhesion or bonding strength between the feedstock layers. Thus, the correlations in figure 5.9 may be caused by poor adhesion between the feedstock layers of the pellets that have the smallest feedstock layers, and are produced with the largest roller gap size. A reason for low adhesion strength could be a decrease of the pellet moisture content, due to increased frictional heating in the die, caused by the increased specific energy consumption of the pellet press, when running with thin feedstock layers and a high roller gap.

Hence, increased drying and poor adhesion between the feedstock layers could also explain the effects of roller gap and feedstock layer on the pellet durability in figure 5.7.

Contribution

From tests using a pilot-scale pellet press, the results are as follows:

- The specific energy consumption of the pellet press is negatively correlated to the thickness of the feedstock layer on the die and is positively correlated to the size of the roller gap.
- The pellet durability is positively correlated to the thickness of the feedstock layer and is negatively correlated to the roller gap size.
- The bulk density of the pellets is negatively correlated to rotational die speed and the size of the roller gap.

- The average pellet length is positively correlated to the thickness of the feedstock layer on the die and is negatively correlated to the size of the roller gap.
- Empirical functions presented for the pellet durability and mass-specific energy consumption of the pellet press were found to match the experimental data.

These findings are applicable to the pellet industry, where the feedstock layer can be used as a parameter to reduce the energy consumption of the pellet press and increase the pellet durability. However, an optimum has yet to be found, since an upper limit of the feedstock layer thickness must exist, related to the size of the die and rollers.

The size of the roller gap should not be above 0.2 mm in terms of optimizing energy consumption and pellet durability. However, eliminating the gap between die and roller could cause significant wear due to direct contact between the rotating parts.

urldate = 01/08/2020,

Chapter 6

Conclusion and Closing Remarks

The gathered conclusion of the studies in this thesis is presented in this chapter.

This thesis considers the effects of die design and process parameters in biomass pelleting. By reviewing the current state-of-the-art, experiments and models have been developed to qualitative and quantitatively analyze selected design and process parameters of the pelleting process.

The main contributions lie within:

- The 1D model for simulation of pelleting pressure in press channels with a conical inlet.
- The literature review in paper B, leading to an identification of research gaps.
- The constitutive model for simulating the viscoplastic behavior of biomass in paper C.
- The CFD model and experimental analysis of feedstock layers in pellets presented in paper D.
- The experimental analysis of the feedstock layers thickness and roller gap size using a pilot-scale pellet press in paper E.

The literature review showed that die parameters, such as the die area and the inlet design of the press channel, are rarely considered in pelleting studies. However, a few studies have indicated that the press channel inlet has a significant effect on energy consumption, and also affect the pellet durability.

The methods for calculation of the pelleting pressure in press channels were found to be based on a set of equations that all utilize the same governing properties of the feedstock and only apply for calculation of the pelleting pressure in a pure cylindrical press channel.

A 1D model was developed, which accounts for the design of the conical press channel inlet. Simulations performed with the 1D model show that the pressure in the press channel peaks at the transition between the press channel inlet and the cylindrical part of the press channel, which also is where the wear is concentrated. Also, the model is capable of simulating the feedstock density and the mass-specific energy consumption, which is calculated from the frictional and compressional work exerted in the press channel. However, the mass-specific energy consumption found from the simulations indicates that the model needs further development due to the overestimation of the frictional work exerted in the press channel. The presented model does not account for the dynamics of the start-stop motion of the feedstock in the press channel, which probably is the main reason for the overestimated energy consumption.

The study of the press channel inlet was continued, by qualitatively analyzing the feedstock layer shapes in pellets produced from continuous single pelleting tests. The layer shapes in pellets produced from dies with different inlet designs were quantified by the kurtosis of the layer shape, which was introduced as a shape factor. The kurtosis was found to correlate with the durability of the pellets and the inlet design of the press channel. Hence, the layer shapes have been shown to compose a link between the inlet design and the pellet durability.

In the study of feedstock layer shapes, the motion of the feedstock in the press channel was simulated using a CFD model, where a simplified Bingham model was utilized to model the feedstock viscosity. The CFD model provides valuable insight to the feedstock motion inside the press channel, and together with the experimental analysis of layer shapes, regions of stagnant feedstock on the inactive part of the die surface were observed together with cases of stagnant feedstock creating a new secondary inlet angle, defined by the interface between moving and stagnant feedstock.

With further investigation, the presented CFD model can form the basis for simulations of larger sections of the die, where the feedstock motion between press channels can be investigated to clarify effects between the die surface and the roller.

Via experimental tests using a pilot-scale pellet press, the effects of the start-stop motion in the press channel were investigated. It was found that the mass-specific energy consumption of the pellet press decreases when the thickness of the feedstock layer on the die is increased, which is equivalent to reducing the number of start-stop movements in the press channel. The trend observed from the experimental results was also shown with a simple

empirical expression of the mass-specific energy consumption based on the static and kinetic friction in the press channel. The results support the idea that the neglected effect of the start-stop motion in the presented 1D model is causing the overestimation of frictional work in the simulations.

The pellet press tests also showed a positive correlation between the thickness of the feedstock layer and the mechanical durability of the pellets. Hence, the thickness of the feedstock layer is considered to be an important parameter in the pelleting process. In the extend of this study, industry-scale tests are ongoing to analyze the effects of the feedstock layer further, and the possibility to reduce the energy consumption of pellet presses.

A Maxwell representation of the SLS constitutive model with two springs and a dashpot was found capable of simulating the visco-plastic behavior of the biomass. A pseudo spring porosity was developed and applied to the SLS Maxwell model for modeling the nonlinear elastic properties of biomass. By fitting the model to experimental compression tests, mechanical properties of spruce with different particle sizes were derived, and one of the model's spring coefficients was found to correlate to the energy required for compressing the biomass. Also, the stress relaxation of the feedstock, quantified by the mass-specific dashpot work, was found to be lowest for pellet produced with small particles, which also had the highest durability.

A trend in the industry of biomass pelleting is that the share of non-woody feedstock used for pellet production is increasing [1], causing a wider variety of the feedstock base, which also is shown by many recent studies of different feedstock types, such as sugarcane bagasse [83], harvest residues of corn [84], lemon trees [85], cassava rhizome [86], tree-leafs [87], and fruit and vegetable waste [88]. Combined with compression tests, the presented constitutive model can be used as a tool for deriving and comparing the mechanical properties of different types of feedstock. With further work, these properties can be applied to the 1D model to simulate die performance and facilitate a quicker design phase for the production of customized die designs for a specific feedstock.

References

[1] C. Calderón, M. Colla, J.-M. Jossart, N. Hemeleers, G. Cancian, N. Aveni, and C. Caferri, "Bioenergy Europe Statistical Report 2019," Bioenergy Europe, Tech. Rep., 2019. [Online]. Available: https://epc.bioenergyeurope.org/wp-content/uploads/2020/02/SR19_Pellet_final-web-1.pdf (Accessed 01/08/2020).

[2] W. Strauss and S. Walker, "Global pellet market outlook in 2018," 2018. [Online]. Available: https://www.canadianbiomassmagazine.ca/pellets/increasing-demand-6705 (Accessed 01/08/2020).

[3] D. Thrän, "Global Wood Pellet Industry and Trade Study 2017," *IEA Bioenergy Task 40*, p. 222, 2017.

[4] European Commision, "A policy framework for climate and energy in the period from 2020 to 2030," 2014.

[5] R. Jonsson and F. Rinaldi, "The impact on global wood-product markets of increasing consumption of wood pellets within the European Union," *Energy*, vol. 133, pp. 864–878, 2017. doi: 10.1016/j.energy.2017.05.178

[6] C. Calderón, G. Gauthier, and J.-M. Jossart, "AEBIOM statistical report 2017 - Full Report," pp. 1–264, 2017. [Online]. Available: https://ibtc.bioenergyeurope.org/aebiom-2017-statistical-report/ (Accessed 01/08/2020).

[7] J. Carter, "Demand for Biomass Pellets and Chips : Japan and South Korea," pp. 1–8, 2016. [Online]. Available: https://blog.forest2market.com/new-opportunities-for-biomass-growth-japan-and-south-korea (Accessed 01/08/2020).

[8] L. Visser, R. Hoefnagels, and M. Junginger, "Wood pellet supply chain costs – a review and cost optimization analysis," *Renewable and Sustainable Energy Reviews*, vol. 118, p. 109506, 2020. doi: https://doi.org/10.1016/j.rser.2019.109506

[9] G. Thek and I. Obernberger, "Wood pellet production costs under austrian and in comparison to swedish framework conditions," *Biomass and Bioenergy*, vol. 27, no. 6, pp. 671 – 693, 2004. doi: https://doi.org/10.1016/j.biombioe.2003.07.007 Pellets 2002. The first world conference on pellets.

[10] "ISO 17225-2:2014, Fuel specifications and classes - Part 2: Graded wood pellets," pp. 1–13, 2014.

[11] European Pellet Council, "ENplus Quality Certification Scheme Part 3: Pellet Quality Requirements," p. 10, 2015. [Online]. Available: https://enplus-pellets.eu/en-in/?option=com_attachments&task=download&id=103:ENplusHandbook_part3_V3 (Accessed 01/08/2020).

[12] N. C. Crawford, A. E. Ray, N. A. Yancey, and N. Nagle, "Evaluating the pelletization of "pure" and blended lignocellulosic biomass feedstocks," *Fuel Processing Technology*, vol. 140, pp. 46–56, 2015. doi: 10.1016/j.fuproc.2015.08.023

[13] D. S. Bajwa, T. Peterson, N. Sharma, J. Shojaeiarani, and S. G. Bajwa, "A review of densified solid biomass for energy production," *Renewable and Sustainable Energy Reviews*, vol. 96, pp. 296 – 305, 2018. doi: https://doi.org/10.1016/j.rser.2018.07.040

[14] I. Obernberger and G. Thek, "Physical characterisation and chemical composition of densified biomass fuels with regard to their combustion behaviour," *Biomass and Bioenergy*, vol. 27, no. 6, pp. 653 – 669, 2004. doi: https://doi.org/10.1016/j.biombioe.2003.07.006 Pellets 2002. The first world conference on pellets.

[15] S. K. Nielsen, M. Mandø, and A. B. Rosenørn, "Review of die design and process parameters in the biomass pelleting process," *Powder Technology*, vol. 364, pp. 971 – 985, 2020. doi: https://doi.org/10.1016/j.powtec.2019.10.051

[16] W. Stelte, J. K. Holm, A. R. Sanadi, S. Barsberg, J. Ahrenfeldt, and U. B. Henriksen, "Fuel pellets from biomass: The importance of the pelletizing pressure and its dependency on the processing conditions," *Fuel*, vol. 90, no. 11, pp. 3285–3290, 2011. doi: 10.1016/j.fuel.2011.05.011

[17] R. Samuelsson, S. H. Larsson, M. Thyrel, and T. A. Lestander, "Moisture content and storage time influence the binding mechanisms in biofuel wood pellets," *Applied Energy*, vol. 99, pp. 109 – 115, 2012. doi: https://doi.org/10.1016/j.apenergy.2012.05.004

[18] N. Kaliyan and R. V. Morey, "Factors affecting strength and durability of densified biomass products," *Biomass and Bioenergy*, vol. 33, no. 3, pp. 337–359, 2009. doi: 10.1016/j.biombioe.2008.08.005

[19] D. Bergström, S. Israelsson, M. Öhman, S. A. Dahlqvist, R. Gref, C. Boman, and I. Wästerlund, "Effects of raw material particle size distribution on the characteristics of Scots pine sawdust fuel pellets," *Fuel Processing Technology*, vol. 89, no. 12, pp. 1324–1329, 2008. doi: 10.1016/j.fuproc.2008.06.001

[20] M. Segerström and S. H. Larsson, "Clarifying sub-processes in continuous ring die pelletizing through die temperature control," *Fuel Processing Technology*, vol. 123, pp. 122–126, 2014. doi: 10.1016/j.fuproc.2014.02.008

[21] T. B. Reed and B. Bryant, *Densified biomass: A new form of solid fuel*. Dept. of Energy, Solar Energy Research Institute, 1978.

[22] R. Jannasch, Y. Quan, and R. Samson, "A Process and Energy Analysis of Pelletizing Switchgrass," Resource Efficient Agricultural Production Canada, Tech. Rep., 2001. [Online]. Available: https://reap-canada.com/online_library/feedstock_biomass/11AProcess.pdf

[23] L. Tabil and S. Sokhansanj, "Process conditions affecting the physical quality of alfalfa pellets," *Applied Engineering in Agriculture*, vol. 12, no. 3, pp. 345–350, 1996. doi: 10.13031/2013.25658

[24] L. Tellefsen, *Handbook in Pelleting Technique (Danish: Håndbog i pilleteringsteknik)*. Esbjerg: Sprout-Matator, 1999.

[25] N. P. K. Nielsen, D. Gardner, T. Poulsen, and C. Felby, "Importance of temperature, moisture content, and species for the conversion process of wood residues into fuel pellets," *Wood and Fiber Science*, vol. 41, no. 4, pp. 414–425, 2009.

[26] J. K. Holm, U. B. Henriksen, J. E. Hustad, and L. H. Sørensen, "Toward an understanding of controlling parameters in softwood and hardwood pellets production," *Energy and Fuels*, vol. 20, no. 6, pp. 2686–2694, 2006. doi: 10.1021/ef0503360

[27] Shi Shuijuan, Wu Kai, Peng Binbin, Wang Shuanhu, and Sun Yu, "Mechanical model and fea of ring die of three-roller pellet mill," in *2010 International Conference on Mechanic Automation and Control Engineering*, 2010, pp. 76–80.

[28] N. P. K. Nielsen, J. K. Holm, and C. Felby, "Effect of fiber orientation on compression and frictional properties of sawdust particles in fuel pellet production," *Energy and Fuels*, vol. 23, no. 6, pp. 3211–3216, 2009. doi: 10.1021/ef800923v

[29] V. I. Osobov, "Theoretical principles of compressing fibrous plant materials," *Trudy Viskhom*, vol. 55, 1967.

[30] M. O. Faborode, "Analysis of extrusion compaction of fibrous agricultural residues for fuel applications," *Biomass*, vol. 21, no. 2, pp. 115–128, 1990. doi: 10.1016/0144-4565(90)90053-M

[31] E. Winter, "Fundamental considerations for preparing densified refuse-derived fuel," U.S. Environmental Protection Agency, Municipal Environmental Research Laboratory, Tech. Rep., 1981.

[32] J. K. Holm, W. Stelte, D. Posselt, J. Ahrenfeldt, and U. B. Henriksen, "Optimization of a multiparameter model for biomass pelletization to investigate temperature dependence and to facilitate fast testing of pelletization behavior," *Energy and Fuels*, vol. 25, no. 8, pp. 3706–3711, 2011. doi: 10.1021/ef2005628

[33] J. K. Holm, U. B. Henriksen, K. Wand, J. E. Hustad, and D. Posselt, "Experimental verification of novel pellet model using a single pelleter unit," *Energy and Fuels*, vol. 21, no. 4, pp. 2446–2449, 2007. doi: 10.1021/ef070156l

[34] M. Puig-Arnavat, J. Ahrenfeldt, and U. B. Henriksen, "Validation of a Multiparameter Model to Investigate Torrefied Biomass Pelletization Behavior," *Energy and Fuels*, vol. 31, no. 2, pp. 1644–1649, 2017. doi: 10.1021/acs.energyfuels.6b02895

[35] S. K. Nielsen, M. Mandø, and A. B. Rosenørn, "1D Model for investigation of energy consumption and wear in die designs used for biomass pelleting," *European Biomass Conference and Exhibition*, vol. 26, pp. 550–558, 2018. doi: 10.5071/26thEUBCE2018-2CO.13.1

[36] R. J. Ross, *Wood handbook : wood as an engineering material*. Department of Agriculture, Forest Service, General Technical Report (GTR), 2010. ISBN 1892529025

[37] P. Zaini, S. Sokansanj, X. Bi, C. J. Lim, S. Mani, S. Melin, and J. Kadla, "Density, heating value, and composition of pellets made from lodgepole pine (Pinus concorta Douglas) infested with mountain pine beetle (Dendroctonus ponderosae hopkins)," *Canadian Biosystems Engineering / Le Genie des biosystems au Canada*, vol. 50, pp. 47–55, 2008.

[38] C. A. Hill and G. A. Ormondroyd, "Dimensional changes in Corsican pine (Pinus nigra Arnold) modified with acetic anhydride measured using a helium pycnometer," *Holzforschung*, vol. 58, no. 5, pp. 544–547, 2004. doi: 10.1515/HF.2004.082

[39] R. M. Kellogg and F. F. Wangaard, "Variation in the cell-wall density of wood," *Wood and Fiber Science*, vol. 1, no. 3, pp. 180–204, 1969.

[40] Andritz Feed & Biofuel, "3D wear measurements of a ring die," Esbjerg, Tech. Rep., 2015.

[41] W. Stelte, C. Clemons, J. K. Holm, J. Ahrenfeldt, U. B. Henriksen, and A. R. Sanadi, "Thermal transitions of the amorphous polymers in wheat straw," *Industrial Crops and Products*, vol. 34, no. 1, pp. 1053–1056, 2011. doi: 10.1016/j.indcrop.2011.03.014

[42] A. S. Olsson and L. Salmen, "Viscoelasticity of Insitu Lignin as Affected by Structure - Softwood vs Hardwood," *ACS Symposium Series*, vol. 489, pp. 133–143, 1992.

[43] S. Z. Chow and K. J. Pickles, "Thermal Softening and Degradation of Wood and Bark," *Wood and Fiber Science*, vol. 3, pp. 166–178, 1971.

[44] L. Salmén, "Viscoelastic properties of in situ lignin under water-saturated conditions," *Journal of Materials Science*, vol. 19, no. 9, pp. 3090–3096, 1984. doi: 10.1007/BF01026988

[45] G. M. Irvine, "The Glass Transitions of Lignin and Hemicellulose and Their Measurement by Differential Thermal-Analysis," *Tappi Journal*, vol. 67, no. 5, pp. 118–121, 1984.

[46] A. Zafari and M. H. Kianmehr, "Factors affecting mechanical properties of biomass pellet from compost," *Environmental Technology (United Kingdom)*, vol. 35, no. 4, pp. 478–486, 2014. doi: 10.1080/09593330.2013.833639

[47] W. Stelte, J. K. Holm, A. R. Sanadi, S. Barsberg, J. Ahrenfeldt, and U. B. Henriksen, "A study of bonding and failure mechanisms in fuel pellets from different biomass resources," *Biomass and Bioenergy*, vol. 35, no. 2, pp. 910–918, 2011. doi: 10.1016/j.biombioe.2010.11.003

[48] L. G. Tabil Jr. and S. Sokhansanj, "Bulk properties of alfalfa grind in relation to its compaction characteristics," *Applied Engineering in Agriculture*, vol. 13, no. 4, pp. 499–505, 1997, cited By :34.

[49] J. S. Tumuluru, C. T. Wright, J. R. Hess, and K. L. Kenney, "A review of biomass densification systems to develop uniform feedstock commodities for bioenergy application," *Biofuels, Bioproducts and Biorefining*, vol. 6, no. 3, pp. 246–256, 2012. doi: 10.1002/bbb

[50] D. J. Gardner and M. Tajvidi, "Hydrogen Bonding in Wood-Based Materials: An update," *Wood and Fiber Science*, vol. 48, no. 4, pp. 234–244, 2016.

[51] C. Macosko, *Rheology: principles, measurements, and applications*, ser. Advances in interfacial engineering series. VCH, 1994. ISBN 978-0-471-18575-8

[52] P. J. Denny, "Compaction equations: A comparison of the Heckel and Kawakita equations," *Powder Technology*, vol. 127, no. 2, pp. 162–172, 2002. doi: 10.1016/S0032-5910(02)00111-0

[53] K. D. Nona, B. Lenaerts, E. Kayacan, and W. Saeys, "Bulk compression characteristics of straw and hay," *Biosystems Engineering*, vol. 118, no. 1, pp. 194–202, 2014. doi: 10.1016/j.biosystemseng.2013.12.005

[54] M. O. Faborode and J. R. O'Callaghan, "Theoretical analysis of the compression of fibrous agricultural materials," *Journal of Agricultural Engineering Research*, vol. 35, pp. 175–191, 1986. doi: 10.1016/S0021-8634(86)80055-5

[55] N. Kaliyan and R. V. Morey, "Constitutive model for densification of corn stover and switchgrass," *Biosystems Engineering*, vol. 104, no. 1, pp. 47–63, 2009. doi: 10.1016/j.biosystemseng.2009.05.006

[56] I. Krycer, D. G. Pope, and J. A. Hersey, "The interpretation of powder compaction data - A critical review," *Drug Dev. Ind. Pharm.*, vol. 9045, no. November, p. 307, 1982. doi: 10.3109/03639048209022103

[57] M. Peleg, "Linearization of relaxation and creep curves of solid biological materials," *Journal of Rheology*, vol. 24, no. 4, pp. 451–463, 1980. doi: 10.1122/1.549567

[58] M. O. Faborode and J. R. O'Callaghan, "Optimizing the compression/briquetting of fibrous agricultural materials," *Journal of Agricultural Engineering Research*, vol. 38, pp. 245–262, 1987. doi: 10.1016/0021-8634(87)90092-8

[59] M. D. Shaw and L. G. Tabil, "Compression, Relaxation, and Adhesion Properties of Selected Biomass Grinds," *Agricultural Engineering International: the CIGR Ejournal*, vol. IX, pp. 1–16, 2007.

[60] N. Mohsenin and J. Zaske, "Stress relaxation and energy requirements in compaction of unconsolidated materials," *Journal of Agricultural Engineering Research*, vol. 21, no. 2, pp. 193–205, 1976. doi: 10.1016/0021-8634(76)90074-3

[61] S. K. Nielsen, H. Rezaei, M. Mandø, and S. Sokhansanj, "Constitutive modelling of compression and stress relaxation in pine pellets," *Biomass and Bioenergy*, vol. 130, p. 105370, 2019. doi: https://doi.org/10.1016/j.biombioe.2019.105370

[62] K. Peleg, "A Rheological Model of Nonlinear Viscoplastic Solids," *Journal of Rheology*, vol. 27, no. 5, pp. 411–431, 1983. doi: 10.1122/1.549714

[63] M. O. Faborode and J. R. O'Callaghan, "A rheological model for the compaction of fibrous agricultural materials," *Journal of Agricultural Engineering Research*, vol. 42, no. 3, pp. 165–178, 1989. doi: 10.1016/0021-8634(89)90048-6

[64] L. Molari, M. Maraldi, and G. Molari, "Non-linear rheological model of straw bales behavior under compressive loads," *Mechanics Research Communications*, vol. 81, pp. 32–37, 2017. doi: 10.1016/j.mechrescom.2017.02.010

[65] M. T. Carone, A. Pantaleo, and A. Pellerano, "Influence of process parameters and biomass characteristics on the durability of pellets from the pruning residues of Olea europaea L," *Biomass and Bioenergy*, vol. 35, no. 1, pp. 402–410, 2011. doi: 10.1016/j.biombioe.2010.08.052

[66] N. Mišljenović, R. Čolović, D. Vukmirović, T. Brlek, and C. S. Bringas, "The effects of sugar beet molasses on wheat straw pelleting and pellet quality. A comparative study of pelleting by using a single pellet press and a pilot-scale pellet press," *Fuel Processing Technology*, vol. 144, pp. 220–229, 2016. doi: 10.1016/j.fuproc.2016.01.001

[67] Y. Li, D. Wu, J. Zhang, L. Chang, D. Wu, Z. Fang, and Y. Shi, "Measurement and statistics of single pellet mechanical strength of differently shaped catalysts," *Powder Technology*, vol. 113, no. 1, pp. 176 – 184, 2000. doi: https://doi.org/10.1016/S0032-5910(00)00231-X

[68] S. Hemamanjushree and V. K. Tippavajhala, "Review Article Simulation of Unit Operations in Formulation Development of Tablets Using Computational Fluid Dynamics," *AAPS PharmSciTech*, vol. 21, no. 3, p. 103, 2020. doi: 10.1208/s12249-020-1635-1

[69] G. Pashos, G. Pantazopoulos, and I. Contopoulos, "A Comprehensive CFD Model for Dual-Phase Brass Indirect Extrusion Based on Constitutive Laws: Assessment of Hot-Zone Formation and Failure Prognosis," *Metals*, vol. 8, no. 12, p. 1043, 2018. doi: 10.3390/met8121043

[70] S. K. Nielsen and M. Mandø, "Experimental and numerical investigation of die designs in biomass pelleting and the effect on layer formation in pellets," 2020.

[71] N. J. Balmforth, I. A. Frigaard, and G. Ovarlez, "Yielding to Stress: Recent Developments in Viscoplastic Fluid Mechanics," *Annual Review of Fluid Mechanics*, vol. 46, no. 1, pp. 121–146, 2014. doi: 10.1146/annurev-fluid-010313-141424

[72] E. C. Bingham, "An Investigation of the Laws of Plastic Flow," *Bulletin of the Bureau of Standards*, vol. 13, no. 2, pp. 309–353, 1916. doi: 10.6028/bulletin.304

[73] ANSYS Inc., "FLUENT user guide, 8.4.5 Viscosity for Non-Newtonian Fluids," 2009.

[74] Y. Liu and J. R. D. Bruyn, "Start-up flow of a yield-stress fluid in a vertical pipe," *Journal of Non-Newtonian Fluid Mechanics*, vol. 257, pp. 50 – 58, 2018. doi: https://doi.org/10.1016/j.jnnfm.2018.03.005

[75] S. K. Kim, "Flow rate based framework for solving viscoplastic flow with slip," *Journal of Non-Newtonian Fluid Mechanics*, vol. 269, pp. 37 – 46, 2019. doi: https://doi.org/10.1016/j.jnnfm.2019.06.002

[76] S. H. Larsson and R. Samuelsson, "Prediction of ISO 17831-1:2015 mechanical biofuel pellet durability from single pellet characterization," *Fuel Processing Technology*, vol. 163, pp. 8–15, 2017. doi: 10.1016/j.fuproc.2017.04.004

[77] R. Shanmugam and C. Rajan, *Skewness and Kurtosis*. John Wiley & Sons, Ltd, 2016, ch. 4, pp. 89–110. ISBN 9781119047063. [Online]. Available: https://onlinelibrary.wiley.com/doi/abs/10.1002/9781119047063.ch4

[78] Dietmar Schulze, *Powders and Bulk Solids Behavior, Characterization, Storage and Flow*. Springer, Berlin, Heidelberg, 2008. ISBN 978-3-540-73767-4

[79] S. K. Nielsen, M. Mandø, and A. B. Rosenørn, "Experimental investigation of feedstock layer thickness and die-roller gap in wood pelleting," in *World Sustainable Energy Days 2020*. Linz/Wels: OÖ Energiesparverband, 2020, pp. 1–10.

[80] K. Wu, S. Shi, W. Ding, B. Peng, and Y. Sun, "Influence of die speed on the energy consumption in the pelleting process," *2010 International Conference on Computing, Control and Industrial Engineering, CCIE 2010*, vol. 1, pp. 247–250, 2010. doi: 10.1109/CCIE.2010.70

[81] "ISO 17828:2015, Solid biofuels — Determination of bulk density," pp. 1–8, 2015.

[82] "ISO17831-1:2015: Solid biofuels; Determination of mechanical durability of pellets and briquettes - Part 1: Pellets," pp. 1–12, 2016.

[83] L. De Almeida, A. Sola, and J. Behainne, "Sugarcane bagasse pellets: Characterization and comparative analysis [pellets de bagaço de cana-de-açúcar: Caracterização e análise comparativa]," *Acta Scientiarum - Technology*, vol. 39, no. 4, pp. 461–468, 2017. doi: 10.4025/actascitechnol.v39i4.30198

[84] D. Djatkov, M. Martinov, and M. Kaltschmitt, "Influencing parameters on mechanical–physical properties of pellet fuel made from corn harvest residues," *Biomass and Bioenergy*, vol. 119, pp. 418–428, 2018. doi: 10.1016/j.biombioe.2018.10.009

[85] M. Dagtekin, G. Gürdil, and B. DemiRel, "Bio-energy potential from lemon orchards," 2019, pp. 109–112.

[86] N. Soponpongpipat, P. Comsawang, and S. Nanetoe, "Quality properties and pyrolysis characteristics of cassava rhizome pellets produced by alternating between pelletizing and torrefaction," *Processes*, vol. 7, no. 12, 2019. doi: 10.3390/PR7120930

[87] L. Clavijo, S. Zlatanovic, G. Braun, M. Bongards, A. Dieste, and S. Barbe, "Eucalyptus kraft lignin as an additive strongly enhances the mechanical resistance of tree-leaf pellets," *Processes*, vol. 8, no. 3, 2020. doi: 10.3390/PR8030376

[88] M. Arulprakasajothi, N. Beemkumar, J. Parthipan, and N. Battu, "Investigating the physio-chemical properties of densified biomass pellet fuels from fruit and vegetable market waste," *Arabian Journal for Science and Engineering*, vol. 45, no. 2, pp. 563–574, 2020. doi: 10.1007/s13369-019-04294-8

Part II

Papers

Paper A

1D Model for Investigation of Energy Consumption and Wear in Die Designs Used for Biomass Pelleting

Simon Klinge Nielsen, Matthias Mandø, and Andreas Brinch Rosenørn

The paper has been published in the
Proceedings of the 26th *European Biomass Conference and Exhibition*, pp. 550–558,
2018

The layout has been revised, and small editorial changes have been made. Content relevant changes, if any, are marked with explicit footnotes.

Paper B

Review of Die Design and Process Parameters in the Biomass Pelleting Process

Simon Klinge Nielsen, Matthias Mandø, and Andreas Brinch Rosenørn

The paper has been published in
Powder Technology Vol. 364, pp. 971-985, 2020.

The layout has been revised.

Paper C

Constitutive Modelling of Compression and Stress Relaxation in Pine Pellets

Simon Klinge Nielsen, Hamid Rezaei, Matthias Mandø, and Shahab Sokhansanj

The paper has been published in
Biomass & Bioenergy Vol. 130, no. 105370, 2019.

The layout has been revised.

Paper D

Experimental and Numerical Investigation of Die Designs in Biomass Pelleting and the Effect on Layer Formation in Pellets

Simon Klinge Nielsen and Matthias Mandø

The paper has been submitted to
Biosystems Engineering (revised paper under review).

The layout has been revised.

Paper E

Experimental Investigation of Feedstock Layer Thickness and Die-Roller Gap in Wood Pelleting

Simon Klinge Nielsen, Matthias Mandø, and Andreas Brinch Rosenørn

The paper has been published in the
Proceedings of the World Sustainable Energy Days, Wels, Austria, March 4-6, pp. 1-10, 2020.

The layout has been revised, and small editorial changes have been made. Content relevant changes, if any, are marked with explicit footnotes.

ISSN (online): 2446-1636
ISBN (online): 978-87-7210-684-7 AALBORG UNIVERSITY PRESS